Thermodynamic description of the plutonium – α–D–isosaccharinic acid system ii: Formation of quaternary Ca(II)–Pu(IV)–OH–ISA complexes

A. Tasi[a,*], X. Gaona[a,**], D. Fellhauer[a], M. Böttle[a], J. Rothe[a], K. Dardenne[a], R. Polly[a], M. Grivé[b], E. Colàs[b], J. Bruno[b], K. Källstrom[c], M. Altmaier[a], H. Geckeis[a]

[a] *Karlsruhe Institute of Technology, Institute for Nuclear Waste Disposal, P.O. Box 3640, 76021 Karlsruhe, Germany*
[b] *Amphos 21 Consulting S.L., Passeig de Garcia i Fària 49-51 1°-1a, E08019 Barcelona, Spain*
[c] *Svensk Kärnbränslehantering AB, Avd. Låg–och medelaktivt Avfall, Evenemangsgatan 13 Box 3091, 169 03 Solna, Sweden*

ARTICLE INFO

Keywords:
Plutonium
Isosaccharinic acid
Calcium
Reducing conditions
Solubility
Thermodynamics
Cementitious materials

ABSTRACT

The quaternary system Ca(II)–Pu(III/IV)–OH–ISA was investigated in a series of solubility experiments where equilibrium conditions were reached from undersaturation conditions with PuO_2(ncr,hyd) at T = (22 ± 2) °C under Ar atmosphere. Experiments were performed in 0.1 m NaCl–NaOH–NaISA–$CaCl_2$ solutions at $8 \leq pH_m \leq 12.5$ ($pH_m = -\log [H^+]$, in molal units), 10^{-5} m $\leq m(ISA)_{tot} \leq 10^{-2}$ m and $10^{-3.5}$ m $\leq m(Ca)_{tot} \leq 0.02$ m. Reducing conditions were adjusted and buffered with hydroquinone (HQ) or Sn(II), which allowed us to work in the (pe + pH_m) region ≈ 9 and ≈ 1.5, respectively.

Solid phase characterization (*in-situ* XRD, XANES and EXAFS) and analogy with the ternary system Pu–OH–ISA previously studied by our group indicate that PuO_2(ncr,hyd) remains unaltered in the course of the solubility experiments at $pH_m \leq 12$ and controls the solubility of Pu under reducing conditions in the presence of ISA and Ca(II). In HQ-systems, the impact of ISA on the solubility of PuO_2(ncr,hyd) is clearly enhanced compared to Ca(II)-free solutions of analogous composition, thus indicating the formation of quaternary complexes of the type Ca(II)–Pu(IV)–OH–ISA in the aqueous phase. The combination of slope analysis of the solubility data and DFT calculations support the predominance of the two aqueous quaternary complexes Ca(II)Pu(IV)$(OH)_3ISA_{-H}^+$ and Ca(II)Pu(IV)$(OH)_3ISA_{-2H}$(aq) below and above $pH_m \approx 11$, respectively. The same speciation scheme explains properly the solubility of Pu in Sn(II)-buffered systems at $pH_m > 11$. Below this pH_m, solubility data under these very reducing conditions suggest the possible formation of ternary Pu(III)–OH–ISA aqueous complexes, although the scatter of the data does not allow a definitive conclusion to be drawn. The presence of Ca(II) in solution destabilizes Pu–ISA colloids, which significantly enhance Pu solubility in comparable, Ca-free systems. Based on these experimental and theoretical results, a thermodynamic model for the system Ca^{2+}–Pu^{4+}–OH^-–Cl^-–ISA^-–H_2O(l) is derived.

This study provides quantitative tools to evaluate the solubility behavior of Pu in reducing cementitious environments containing ISA, as expected in underground repositories for low- and intermediate-level radioactive waste (L/ILW) due to the degradation of cellulosic materials.

1. Introduction

This second contribution to our series "Thermodynamic description of the plutonium – α–D–isosaccharinic acid system" aims at quantitatively evaluating the impact of calcium on the solubility and complexation phenomena of the binary system under alkaline, reducing conditions. It complements and further extends our previous work on the "*Thermodynamic description of the plutonium – α–D–isosaccharinic acid system. I: Solubility, complexation and redox behavior in NaCl–NaISA–NaOH systems*" by Tasi et al. (2018a). In our first contribution, we reported that α–D–isosaccharinic acid (HISA) forms strong complexes with plutonium (Pu(IV)$(OH)_3ISA_{-H}^-$, Pu(IV)$(OH)_3ISA_{-2H}^{2-}$ and Pu(III)$(OH)ISA_{-H}$(aq)) under alkaline, reducing aqueous conditions. The formation of these complexes largely enhances the solubility of PuO_2(ncr,hyd), where "ncr" and "hyd" designate the nanocrystalline and hydrated character of the Pu(IV) solid phase used. Beyond these monomeric complexes, we also provided evidence on the formation and stability of so far undefined "Pu–ISA colloids". These colloidal moieties

* Corresponding author.
** Corresponding author.
E-mail addresses: agost.tasi@kit.edu (A. Tasi), xavier.gaona@kit.edu (X. Gaona).

led to a systematic increase of the solubility of PuO_2(ncr,hyd) by ≈2 log_{10}-units.

Calcium is a relevant component in cementitious systems, where portlandite ($Ca(OH)_2$) and calcium silicate hydrates (C-S-H phases) largely control the pore water composition in the degradation stages II and III of cement. These solid phases impose hyperalkaline conditions ($10 \leq pH \leq 12.5$) over long time periods and result in relatively high calcium concentrations in solution (1 mM ≤ $[Ca]_{aq}$ ≤ 20 mM) (Berner, 1992; Taylor, 1997; Wieland and Van Loon, 2002). Under these conditions, calcium can have a strong impact the solution chemistry of the Pu–ISA system: (i) decreasing the concentration of free ligand ($[ISA]_{free}$), and (ii) enhancing the stability of Pu(III/IV)–OH–ISA complexes (*e.g.* promoting the formation of stable quaternary complexes Ca–Pu(III/IV)–OH–ISA).

A large number of experimental studies have investigated the complexation of ISA with Ca(II) (Rai et al., 1998; Van Loon et al., 1999, 2004; Vercammen et al., 1999a; Vercammen, 2000; Rai et al., 2003; Van Loon et al., 2004; Dudas et al., 2017). These publications agree in the definition of two main aqueous complexes, namely $CaISA^+$ and $CaISA_{-H}$(aq). The latter complex gains relevance under hyperalkaline pH conditions, and involves the deprotonation of an alcohol group of ISA (either C2 or C4) as recently described in (Dudas et al., 2017). The precipitation of $Ca(ISA)_2$ (cr) controls the total concentration of ISA in Ca-containing solutions (Van Loon et al., 1999; Keith-Roach et al., 2014) for instance buffering $[ISA]_{tot}$ ≈ 20 mM under porewater conditions corresponding to the degradation stage II of cement (pH = 12.5, $[Ca]_{tot}$ = 20 mM). The critical reviews of available experimental studies and corresponding selection of thermodynamic data for the system Ca(II)–ISA conducted by Hummel et al. (2005) and by Rai and Kitamura (2015) are summarized in Table A3 in the Appendix and were considered in the data evaluation in the present work.

For tetravalent actinides, the possible formation of very stable quaternary complexes of the type Ca(II)–An(IV)–OH–L, where An = Th with L = ISA as well as with α-D-gluconate (HGLU, a similar alpha-hydroxycarboxylic acid, with expectedly comparable complexation properties) has been controversially discussed in the literature, mostly based upon sorption (Vercammen et al., 2001; Tits et al., 2002, 2005; Wieland et al., 2002; Tits et al., 2005) and solubility (Randall et al., 2013; Colàs, 2014) studies. The formation of such complexes can be rationalized by the expected interaction (stabilization) of negatively charged species (*e.g.* ternary An(IV)–OH–ISA complexes) with Ca^{2+}. Indeed, a number of examples involving the interaction of Ca^{2+} with negatively charged moieties have been also reported for other (actinide) systems, *e.g.* $Ca_xUO_2(CO_3)_3^{2x-4}$ (with x = 1–2 (Kalmykov and Choppin, 2000; Bernhard et al., 2001; Lee and Yun, 2013; Endrizzi and Linfeng, 2014), among others), $Ca_xNpO_2(OH)_y^{1+2x-y}$ (with x = 1 or 3 and y = 2 or 5 (Fellhauer et al., 2016a; Fellhauer et al., 2016b),) or $Ca_4An(OH)_8^{4+}$ (with An = Th(IV), Np(IV) and Pu(IV) (Altmaier et al., 2008; Fellhauer et al., 2010)). A short summary of the main studies focusing on the system Ca(II)–Th(IV)–OH–ISA is provided below.

Vercammen and co-workers (Vercammen et al., 1999b, 2001; Vercammen et al., 1999b; Vercammen, 2000; Vercammen et al., 2001) investigated the sorption of ^{234}Th(IV) onto different materials (feldspar, polyallomer, BioRad) in the presence of ISA (10^{-8} – 10^{-2} M) and Ca(II) ions ($7{\cdot}10^{-4}$ – $1.8{\cdot}10^{-3}$ M) in the pH-range 10.7–13.3 (at I = 0.3 M, $NaClO_4$). Based on slope analysis of their sorption data (log $[Th]_{tot}$ *vs.* pH, log $[Th]_{tot}$ *vs.* log $[ISA]_{tot}$, and log $[Th]_{tot}$ *vs.* log $[Ca]_{tot}$), the authors proposed the formation of the quaternary complex Ca(II)Th(IV)$(OH)_4(ISA)_2$(aq) and determined the corresponding equilibrium constant. Analogous experiments conducted by these authors with ^{152}Eu disregarded the formation of quaternary complexes Ca(II)–Ln(III)–OH–ISA within the investigated conditions.

Tits, Wieland and co-workers (Tits et al., 2002, 2005) investigated the sorption of ^{228}Th(IV) onto calcite and hardened cement paste in the presence of ISA and GLU. Experiments were conducted with artificial cement porewater (pH = 13.3; $[Ca]_{tot}$ ~$1.6{\cdot}10^{-3}$ M). Special care was taken to avoid the formation of colloidal species, and the possible sorption of ISA/GLU onto the solid phases was thoroughly evaluated. Due to boundary conditions set in their experiments (constant pH and $[Ca]_{tot}$), the authors could not evaluate the stoichiometry of the Th(IV)–ISA complex/es forming, and assumed the predominance of the complex Ca(II)Th(IV)$(OH)_4(ISA)_2$(aq) as previously proposed by Vercammen et al. (2001).

Randall et al. (2013) performed solubility experiments with ThO_2(am) in the presence of ISA in alkaline solutions previously equilibrated with $Ca(OH)_2$(s) at pH ≈ 9 and 12. Unfortunately, the authors did not report $[Ca]_{tot}$ after the corresponding equilibration with $Ca(OH)_2$(s), and thus this parameter remains ill-defined in the evaluation of their results. Slope analysis of their solubility data indicated the formation of a complex with a Th(IV):ISA ratio of 1:2. The calculation of the solubility of ThO_2(am) using the equilibrium constant reported in the work of Vercammen et al. (2001) for the complex CaTh$(OH)_4(ISA)_2$(aq) resulted in a large overestimation of the experimental observations. The concentration of Ca used in such calculations was not indicated (Randall et al., 2013). In a similar context but using GLU instead of ISA, Colàs (2014) reported a similar impact of GLU in the solubility of Th(IV) in the absence and presence of Ca(II), thus challenging the formation of quaternary Ca(II)–Th(IV)–OH–GLU complexes previously reported in the study by Tits et al. (2005).

The possible formation of quaternary complexes Ca(II)–An(IV)–OH–ISA has relevant implications in the context of repositories for the disposal of L/ILW, where large amounts of ISA (through cellulose degradation) and Ca(II) (present in cementitious materials) can be present. Thermodynamic calculations using data on the quaternary complex Ca(II)Th(IV)$(OH)_4(ISA)_2$(aq) as reported by Vercammen et al. (2001); Tits et al. (2002); Wieland et al. (2002); Tits et al. (2005) result in a significant enhancement of the solubility of Th(IV) in cementitious environments. The possible formation of analogous complexes with other tetravalent actinides could have a significant impact in the calculation of the source term of key radionuclides such as Pu. In this context, we have systematically investigated the system Ca(II)–Pu(III/IV)–OH–ISA with a combined approach using solubility experiments under controlled redox conditions, extensive solid phase characterization and density functional theory (DFT) calculations. This study aims at providing robust solubility upper limits for the estimation of the source term in conditions relevant for the disposal of L/ILW, and further to derive chemical and thermodynamic models that can be implemented in thermodynamic databases (TDB) and geochemical calculations.

2. Experimental section

Experiments with plutonium were performed in specialized laboratories in the controlled area of KIT–INE. All experiments were conducted in Ar gloveboxes with O_2 concentration significantly below 10 ppm. The same experimental approach as described in Tasi et al. (2018a) was applied for the investigation of the quaternary Ca(II)–Pu–OH–ISA system. The reader is referred to our previous contribution for a detailed description on (i) pH and E_h measurements; (ii) characterization of the aqueous phase; (iii) characterization of the solid phase; (iv) data evaluation and methods for thermodynamic modelling; and (v) DFT calculations.

2.1. Chemicals

Solutions were prepared with ultra–pure water purified with a Milli–Q apparatus (Millipore, 18.2 MΩ, 22 ± 2 °C). Before use, Milli–Q water was boiled for several hours and simultaneously purged with Ar gas to remove traces of dissolved CO_2(g). Standard chemicals, NaISA (0.16 ± 0.02 M) and ^{242}Pu (with 99.4 wt. % ^{242}Pu) stock solutions were obtained or synthesized as described in Tasi et al. (2018a). $CaCl_2{\cdot}2H_2O$ (p.a.) was obtained from Merck. Carbonate impurity in

1.0 M NaOH Titrisol (Merck) was quantified as $(3 \pm 1)\cdot10^{-5}$ M, as described in Tasi et al. (2018a).

2.2. Solubility experiments

The system Ca(II)–Pu(III/IV)–OH–ISA was investigated in six series of independent batch solubility experiments (with total volumes of 25 mL each) where equilibrium conditions were reached from undersaturation conditions. Redox conditions were set with 2 mM of either hydroquinone (HQ) or Sn(II). Solutions at pH_c = 8 and 9 were buffered with 20 mM of TRIS and CHES, respectively. The ionic strength of the solutions was kept constant at 0.10 M with NaCl. Three series of solubility experiments were prepared in the presence of HQ or Sn(II):

1 pH_c varying from 8 to 12.4, with [ISA] = constant = $1\cdot10^{-3}$ M and $[Ca]_{tot}$ = constant = 0.01 M.

2. [ISA] varying from $1\cdot10^{-5}$ to 0.01 M, with pH_c = constant = 12 and $[Ca]_{tot}$ = constant = 0.01 M.

3 $[Ca]_{tot}$ varying from $3\cdot10^{-4}$ to 0.02 M, with pH_c = constant = 12 and
[ISA] = constant = $1\cdot10^{-3}$ M.

Before the addition of the plutonium solid phase, pH_c values of the matrix solutions were adjusted with HCl and NaOH solutions of same ionic strength until constant pH_c and E_h readings were attained. The concentration ranges considered for Ca(II) and ISA were based upon preliminary calculations based on the thermodynamic data summarized in Tables A2 and A3 given in the Appendix. Special attention was taken to strictly maintain constant ionic strength (I = 0.10 M NaCl–NaOH–-NaISA–$CaCl_2$) within the series and to avoid the precipitation of Ca$(ISA)_2$(s) and/or Ca$(OH)_2$(s) phases. Although both phases were calculated to be undersaturated in the experimental conditions, $[Ca]_{tot}$ and $[ISA]_{tot}$ of selected samples with high initial concentrations of Ca(II) or ISA were quantified after two weeks of equilibration time using inductively coupled plasma–optical emission spectroscopy (ICP–OES, Optima 8300 DV, Perkin Elmer) and total organic carbon measurements (TOC, Shimadzu TOC5000), respectively. In all cases, $[Ca]_{tot}$ and $[ISA]_{tot}$ remained virtually the same as the initial values (within the analytical precision, $\sim \pm$ 5%), thus confirming the absence of any precipitation process.

After achieving constant readings of pH_c and E_h, approximately 0.25 mg of an aged (for *ca.* 8 years in 0.10 M NaCl solution), nanocrystalline Pu(IV)O_2 (ncr,hyd) solid phase were added to each individual batch sample. The structural properties and solubility behaviour (in the absence of ISA and Ca(II)) of the initially used Pu solid phase are published elsewhere (Tasi et al., 2018b). Larger amounts (1.5 – 2.5 mg) of the same solid phase were introduced to selected samples with pH_c = 12 (for both, HQ- and Sn(II)-buffered systems) allowing for an extensive solid phase characterization by *in-situ* XRD, XANES and EXAFS (see Tasi et al. (2018a) for details). After the addition of the Pu solid phase, concentrations of Pu, pH_c and E_h in each sample were regularly monitored for up to 102 days. Phase separation was performed by ultrafiltration with 10 kD ($\sim$2 nm) filters or by ultracentrifugation at 90000 rpm (694000 g) for 1 h (see further details in Tasi et al. (2018a)).

Similar values of $[Pu]_{tot}$ were obtained with both phase separation methods, and both datasets are plotted without further differentiation if the solubility plots shown in Section 3. The concentration of Pu in the supernatant without any phase separation was measured for selected samples to evaluate the possible presence of colloidal Pu species. Equilibrium conditions (assumed after constant pH_c, E_h and $[Pu]_{tot}$ values) were normally attained within 30 days of contact time. Detected concentrations in molar units (*e.g.* $[Pu]_{tot}$, expressed in M) were converted to the molal scale ($m(Pu)_{tot}$, expressed in mol·kg_w^{-1}) using the conversion factors reported in NEA–TDB (Guillaumont et al., 2003).

2.3. Theoretical methods

In the theoretical part of this study we applied the same methodology as presented previously (see Tasi et al., 2018a). The structures of the identified Ca(II)–Pu(IV)–OH–ISA complexes were investigated by means of DFT calculations (Hohenberg and Kohn, 1964; Kohn and Sham, 1965). The calculations were performed using TURBOMOLE (version 7.0, 2015) (Schäfer et al., 1992; Eichkorn et al., 1995; Treutler and Ahlrichs, 1995; Eichkorn et al., 1997; von Arnim and Ahlrichs, 1999; Deglmann et al., 2004; Ahlrichs et al., 2015) with the same functional and basis set as in our previous report (DFT-BP86 (Ahlrichs et al., 2000), def2-SVP (Schäfer et al., 1992)). For Pu(IV) (Moritz et al., 2007), we used the 5f-in core pseudo potentials (PP) which considerably simplified the DFT calculations (see Tasi et al. (2018a) for further details).

In the course of the process, the formerly obtained ternary species of the Pu(IV)–OH–ISA system (adapted from Tasi et al., 2018a) were taken as the basis and one Ca^{2+} ion was added to each structure to be optimized. In aqueous solutions, Ca(II) is surrounded by eight water molecules in the first coordination shell, thus, we accordingly added eight additional water molecules to the system to account for a proper saturation of Ca(II) in the complex. Firstly, DFT calculations were performed without the addition of any solvent, corresponding to a calculation in the gas phase. Further calculations including aqueous media approximated with the conductor-like screening model (COSMO) (Klamt, 1995; Klamt and Schuurmann, 1997) were also executed. Considering the first water shell explicitly and dealing with additional solvation effects by means of COSMO provides a reasonable approach to investigate structures of species in aqueous solutions.

3. Results and discussion

3.1. Solubility experiments

Experimental pH_m and E_h (converted to pe) values of all solubility samples are shown in the Pourbaix diagram of Pu in Figure A1 of the Appendix. All investigated systems featured stable pH_m ($\pm$ 0.05) and E_h ($\pm$ 15 – 30 mV, depending upon pH-region) readings over the time frame of this study ($\sim$3 months). Measured (pe + pH_m) values are consistent with our previous solubility studies in the absence of ISA (Tasi et al., 2018b) and in the presence of ISA but absence of Ca(II) (Tasi et al., 2018a). As in both previous studies, the HQ-buffered system (with redox conditions clearly in the Pu(IV) predominance field, see A1) is considered as the reference case to evaluate the interaction of Pu (IV) with ISA in the presence of Ca(II). Although Pu(IV) expectedly dominates the solution chemistry of plutonium also in Sn(II)-buffered systems featuring more reducing redox conditions, the possible contribution of Pu(III) (especially in less alkaline conditions) must be accounted for in the evaluation of the solubility.

The solubility of PuO_2(ncr,hyd) measured in the presence of ISA and Ca is shown in Figs. 1–3:

i. as a function of pH_m (with constant $m(ISA)_{tot}$ and $m(Ca)_{tot}$, Fig. 1a and b),
ii. as a function of log $m(ISA)_{tot}$ (with constant pH_m and $m(Ca)_{tot}$, Fig. 2), and
iii. as a function of log $m(Ca)_{tot}$ (with constant pH_m and $m(ISA)_{tot}$, Fig. 3).

All figures include also the solubility of PuO_2(ncr,hyd) (i) in the absence of ISA and Ca(II), and (ii) in the presence of ISA and absence of Ca(II), calculated for the same experimental conditions using the chemical and thermodynamic models summarized in Tables A1, A4 and A5 of the Appendix.

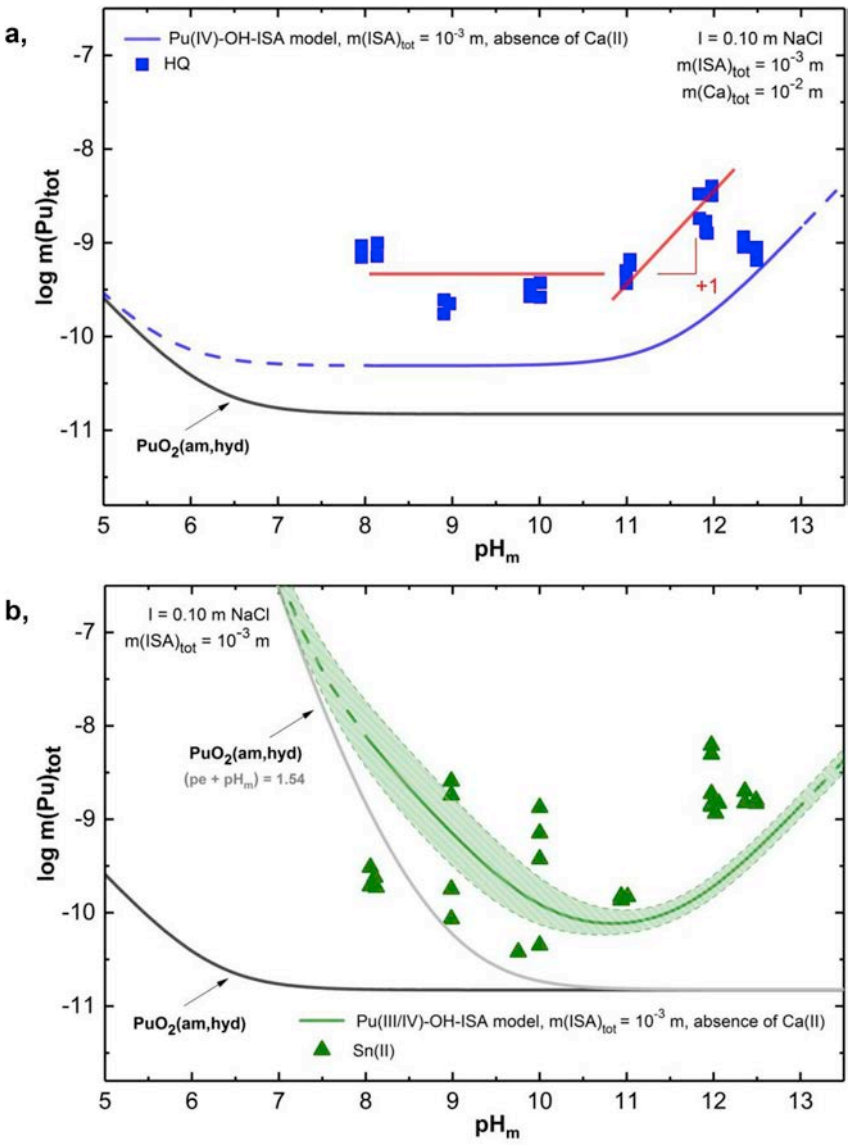

Fig. 1. Experimentally measured $m(Pu)_{tot}$ in equilibrium with PuO_2(ncr,hyd) in 0.10 m NaCl at $m(ISA)_{tot} = 10^{-3}$ m and $m(Ca)_{tot} = 0.01$ m with $pH_m = 8 - 12.4$ (a) in HQ-systems (■), and (b) in Sn(II)-systems (▲). Blue and green lines (solid and dashed) correspond to the solubility of PuO_2(ncr,hyd) calculated for the same boundary conditions but absence of Ca(II). Green shaded area is accounting for the uncertainties in the thermodynamic data and the parameter: $(pe + pH_m) = (1.54 \pm 0.14)$. Black and grey solid lines correspond to the solubility of PuO_2(ncr,hyd) calculated for the same boundary conditions but absence of ISA and Ca(II). Calculations were conducted using thermodynamic data summarized in Tables A1–A5 of the Appendix. (For interpretation of the references to colour in this figure legend, the reader is referred to the Web version of this article.)

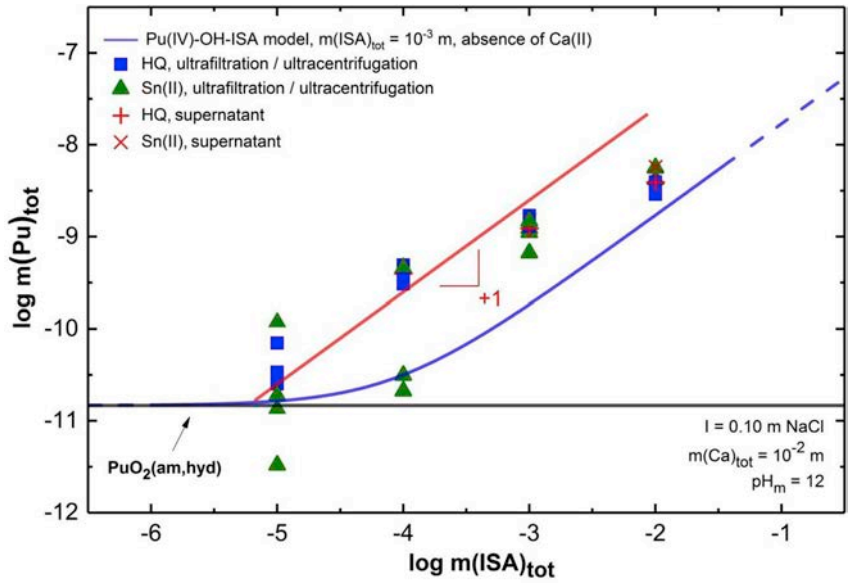

Fig. 2. Experimentally measured $m(Pu)_{tot}$ in equilibrium with PuO_2(ncr,hyd) in 0.10 m NaCl at $pH_m = 12$ and $m(Ca)_{tot} = 0.01$ m conditions with 10^{-5} m $\leq m(ISA)_{tot} \leq 10^{-2}$ m in HQ- (■) or Sn(II)-buffered solutions (▲). Cross symbols are the total concentrations of Pu in the supernatants (sampled without any phase separation) of the Sn(II)- (x) and HQ- (+) systems. Blue lines (solid and dashed) correspond to the solubility of PuO_2(ncr,hyd) calculated for the same boundary conditions but absence of Ca(II). Black solid line corresponds to the solubility of PuO_2(ncr,hyd) calculated in the absence of ISA and Ca(II). Calculations conducted using thermodynamic data summarized in Tables A1–A5 of the Appendix. (For interpretation of the references to colour in this figure legend, the reader is referred to the Web version of this article.)

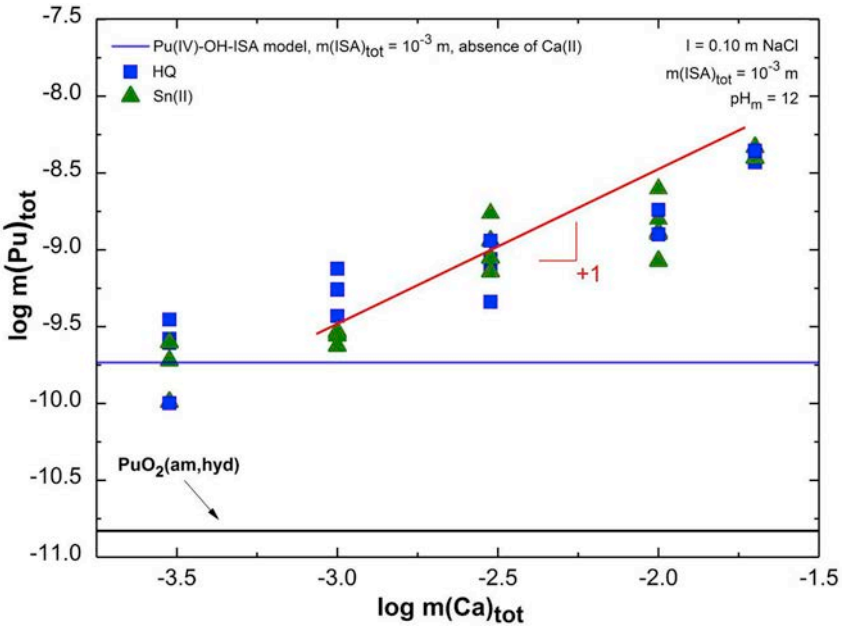

Fig. 3. Experimentally measured $m(Pu)_{tot}$ in equilibrium with PuO_2(ncr,hyd) in 0.10 m NaCl at $pH_m = 12$ and $m(ISA)_{tot} = 10^{-3}$ m, with $3{\cdot}10^{-4}$ m $\leq m(Ca)_{tot} \leq 10^{-3}$ $2{\cdot}10^{-2}$ m, in HQ- (■) or Sn(II)-buffered solutions (▲). Blue solid line corresponds to the solubility of PuO_2(ncr,hyd) calculated for the same boundary conditions but absence of Ca(II). Black solid line shows the solubility of PuO_2(ncr,hyd) calculated in the absence of ISA and Ca(II). Calculations conducted using thermodynamic data summarized in Tables A1–A5 of the Appendix. (For interpretation of the references to colour in this figure legend, the reader is referred to the Web version of this article.)

3.1.1. Solubility of PuO_2(ncr,hyd) at constant $m(ISA)_{tot}$ and $m(Ca)_{tot}$ with $8 \leq pH_m \leq 12.4$

Fig. 1a shows a clear and systematic increase in the solubility of PuO_2(ncr,hyd) in HQ-systems (■) with $m(ISA)_{tot} = 10^{-3}$ m and $m(Ca)_{tot} = 0.01$ m, compared to the solubility of the ternary Pu(IV)–OH–ISA system in the absence of Ca(II) (blue line in the figure). This observation strongly supports the formation of quaternary Ca(II)–Pu(IV)–OH–ISA aqueous complexes in HQ-systems. For this redox system, same/similar pH_m-dependency of the solubility is observed in the absence and presence of Ca(II), suggesting that Pu(IV)–ISA complexes in the presence of Ca(II) hold similar Pu:OH ratios in their stoichiometries as those reported in the absence of Ca(II): 1:4 and 1:5. However, a decrease in the solubility of PuO_2(ncr,hyd) is observed at $pH_m = 12.4$, compared to $m(Pu)_{tot}$ measured at $pH_m \approx 12$. This observation is further discussed below in connection with the slope analysis of the solubility data.

More scattered solubility data are obtained in Sn(II)-buffered systems (Fig. 1b) compared to HQ-systems (Fig. 1a). The solubility of PuO_2(ncr,hyd) in Sn(II)-buffered systems at $pH_m > 10$ is clearly above the calculated solubility in the absence of Ca(II) (green line in the figure), and generally agrees with the solubility determined in HQ-systems. This observation suggests that the same equilibrium reaction controls the solubility of plutonium in both systems. Similar results were obtained in our previous solubility study in the presence of ISA but absence of Ca(II) (Tasi et al., 2018a). Solubility data in Sn(II)-buffered systems at $pH_m \leq 10$ show a large uncertainty, especially within $pH_m = 9 - 10$. In this pH_m-range, $m(Pu)_{tot}$ scatter around the calculated solubility of PuO_2(ncr,hyd) in Sn(II)-buffered systems with ISA and absence of Ca(II), which may support the absence of quaternary species forming between Ca(II) and the Pu(III) complex $Pu(III)(OH)ISA_{-H}(aq)$ reported in Tasi et al. (2018a). This hypothesis is in line with results of previous studies with Eu(III)–ISA (Vercammen et al., 2001; Randall et al., 2013) and Nd(III)/Cm(III)–ISA (Gugau, 2016; Gaona et al., 2017), which disregarded the formation of analogous quaternary Ca(II)–Ln(III)/An(III)–OH–ISA complexes. Due to the inconclusive solubility data in Sn(II)-buffered systems, the development of a thermodynamic model for quaternary system Ca(II)–Pu–OH–ISA is entirely based on the solubility data in HQ-buffered systems and thus restricted to Pu(IV).

Taking into consideration the limitations in the solubility data obtained in Sn(II)-buffered -systems, the following slope analysis can be outlined for the solubility of Pu in HQ-buffered solutions (Fig. 1a):

i. $pH_m = 8 - 11$: as in the absence of Ca(II) (see (Tasi et al., 2018a)), a clear and pH_m-independent enhancement in Pu solubility is observed. This indicates that, within this pH_m-range, no protons are involved in the equilibrium reaction controlling the solubility of Pu in the presence of ISA and Ca(II).
ii. $pH_m = 11 - 12$: a pH_m-dependent increase of the solubility is observed, with a slope ($\log m(Pu)_{tot}$ *vs.* pH_m) of $\approx +1$. This finding suggests that one H^+ is released in the equilibrium reaction controlling the solubility of Pu. A similar behavior can be claimed for the solubility of Pu in Sn(II)-systems (Fig. 1b). Note however that because of the limited number of experimental points defining this pH_m-region, a slope of $+2$ (with the corresponding implications in the stoichiometry Pu:OH in the Ca-Pu-ISA complex) could also explain the available solubility data. This option was also tested to in the development of a thermodynamic model in Section 3.2.
ii. $pH_m = 12.4$: experimental data shows a clear decrease in the solubility of Pu with respect to the sample at $pH_m = 12$. A similar behavior is observed for the solubility of Pu in the Sn(II)-buffered systems. Indeed, the solubility data at this pH_m value is very similar to the solubility in the absence of Ca(II). TOC and ICP-OES measurements performed after 2 weeks of equilibration of the inactive system (before the addition of Pu solid phases) indicated that no loss of ISA and/or Ca(II) took place. These observations would indicate the possible formation of a quaternary Ca(II)–Pu–OH–ISA solid phase, although so far no conclusive evidence is available in this respect. Solubility data obtained in the presence of Ca(II) at $pH_m = 12.4$ were disregarded in the development of the thermodynamic model for the system Ca(II)–Pu(IV)–OH–ISA in Section 3.2.

3.1.2. Solubility of PuO_2(ncr,hyd) at constant pH_m and $m(Ca)_{tot}$ with $-5 \leq \log m(ISA)_{tot} \leq -2$

A clear and systematic enhancement in the solubility of PuO_2(ncr,hyd) is observed with increasing $m(ISA)_{tot}$ at constant pH_m (12.0) and $m(Ca)_{tot}$ (10^{-2} m) (Fig. 2). The trend is very similar in HQ- and Sn(II)-buffered systems, suggesting that the equilibrium reactions controlling the solubility of Pu are the same and involve Pu(IV)–ISA complexes in both cases. The clear increase in the solubility with respect to the Ca(II)-free system (solid blue line in Fig. 2) supports again the formation of a quaternary Ca(II)–Pu(IV)–OH–ISA complexes.

Although the formation of binary/ternary Ca(II)–OH–ISA complexes ($CaISA^+$ and CaOHISA(aq)) must be taken into account in the interpretation of the data due to the decrease in $m(Ca^{2+})_{free}$ and $m(ISA^-)_{free}$, a slope of +1 (log $m(Pu)_{tot}$ *vs.* log $m(ISA)_{tot}$ and thus a stoichiometry Pu:ISA of 1:1) can be postulated both for HQ- and Sn(II)-systems. Note, however that the solubility data obtained for the highest ISA concentration (log $m(ISA)_{tot} = -2$) slightly deviates from this trend (although precipitation of both $Ca(OH)_2$(s) and $Ca(ISA)_2$(s) can be excluded in the system).

Pu(IV) "colloidal species" were found to play an important role enhancing the solubility of PuO_2(ncr,hyd) in the presence of ISA but absence of Ca(II) (Tasi et al., 2018a). In the present study, however, m $(Pu)_{tot}$ determined in the supernatant without phase separation (red cross symbols in Fig. 2) were the same as $m(Pu)_{tot}$ measured after ultracentrifugation or ultrafiltration. The data highlight the relevant role of Ca(II) in the destabilization of "Pu(IV)–ISA colloids". We note that a similar behaviour is known for clay colloid suspensions, where the presence of Ca(II) can cause the gradual agglomeration of the colloidal particles due to the ion exchange of Li^+ and Na^+ ions by Ca^{2+} at the charged basal clay planes (Bouby et al., 2011). The critical coagulation concentration (CCC) of Ca^{2+} ions for destabilizing clay colloid suspensions is known to lie at 10^{-3} M (Bouby et al., 2011). Ca^{2+} ions are also well known to act as a coagulating agent for organic humic colloids due to its very effective screening of surface charges (Weng et al., 2002).

3.1.3. Solubility of PuO_2(ncr,hyd) at constant pH_m and $m(ISA)_{tot}$ with $-3.5 \leq \log m(Ca)_{tot} \leq -1.7$

Fig. 3 shows a clear increase in the solubility of plutonium with increasing $m(Ca)_{tot}$ at constant pH_m (12) and $m(ISA)_{tot}$ (10^{-3} m). Virtually the same trend in the solubility is observed for HQ- and Sn(II)-buffered systems, suggesting again that the equilibrium reactions controlling the solubility of Pu under these conditions are the same and involve the participation of Pu(IV)-ISA complexes in both systems.

The increase of log $m(Pu)_{tot}$ with increasing log $m(Ca)_{tot}$ follows a slope $\approx +1$, indicating that the Ca:Pu ratio of the Pu–ISA complex forming at $pH_m = 12$ is 1:1. For the lowest concentration of Ca(II) (log $m(Ca)_{tot} = -3.5$), solubility data are in excellent agreement with the concentration of plutonium calculated for the same $m(ISA)_{tot}$ but in the absence of Ca(II). This indicates that the effect of Ca(II) disappears at this concentration level, and provides further confidence in the thermodynamic model previously derived in our first publication for the system Pu^{3+}–Pu^{4+}–OH^-–Cl^-–ISA^-–H_2O(l) (Tasi et al., 2018a).

3.1.4. Solid phase characterization

3.1.4.1. Synchrotron-based in-situ XRD. Fig. 4 shows the *in-situ* XRD patterns collected from the solid phases controlling the solubility of Pu in HQ- and Sn(II)-systems, equilibrated in solutions with m $(ISA)_{tot} = 10^{-3}$m, $m(Ca)_{tot} = 0.01$m at $pH_m = 12$ for 150 days. The figure also shows the diffractogram of the empty double containment used in the course of the synchrotron-based measurements at the INE–Beamline at KARA.

XRD patterns obtained in both HQ- and Sn(II)-buffered systems are in excellent agreement with the reference pattern of PuO_2(cr) reported by Zachariansen (1949). These observations also agree with the results obtained in the presence of ISA but absence of Ca(II) (see (Tasi et al., 2018a)), thus supporting that in both cases the initial characteristics of PuO_2(ncr,hyd) is retained in the presence of ISA. The absence of any diffraction pattern belonging to $Ca(ISA)_2$ (cr) (detection limit at ~5–10%, see Rai et al. (1998) and Tasi et al. (2018a)) confirms that this binary solid phase does not precipitate under the conditions of our experiments. This underlines our previous quantitative analysis and it is in agreement with calculations using thermodynamic data summarized in the Appendix.

3.1.4.2. XANES. Pu L_{III}–edge XANES spectra collected for the solid phases recovered from solubility experiments in HQ- and Sn(II)-buffered systems with $m(ISA)_{tot} = 10^{-3}$ m, $m(Ca)_{tot} = 10^{-2}$ m and $pH_m = 12$ (t_{eq} = 150 days) are shown in Fig. 5. The figure also includes the XANES spectra of PuO_2(ncr,hyd) "Pu starting material" (see (Tasi et al., 2018b)) and the reference spectra reported by Brendebach and co-workers (Brendebach et al., 2009) for aqueous Pu(III) and Pu(IV) species under acidic conditions.

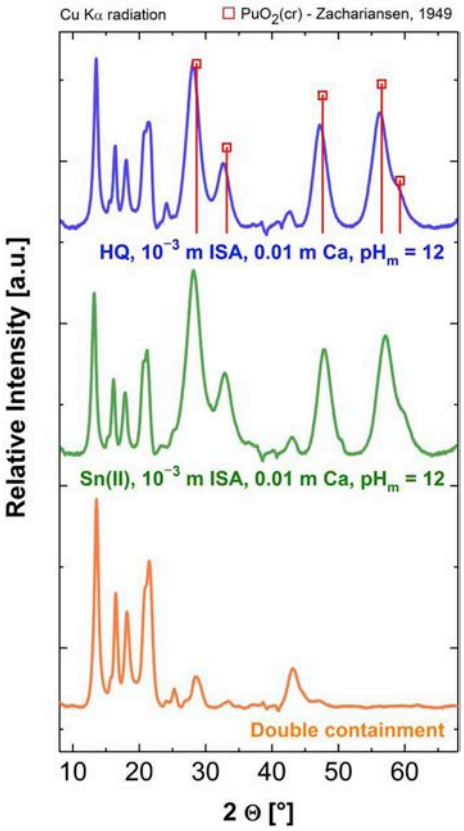

Fig. 4. *In-situ* XRD patterns collected at the INE-Beamline at KARA for the Pu solid phases recovered from HQ-buffered (blue, top) and Sn(II)-buffered (green, middle) solubility experiments with $m(ISA)_{tot} = 10^{-3}$ m, $m(Ca)_{tot} = 10^{-2}$ m and $pH_m = 12$ (t_{eq} = 150 days). The lower diffractogram in orange corresponds to the empty double containment used for the in-situ measurements. Squares indicate peak positions and relative intensities reported for PuO_2(cr) (Zachariansen, 1949). (For interpretation of the references to colour in this figure legend, the reader is referred to the Web version of this article.)

The edge energies of the XANES spectra collected for all the investigated Pu solid phases are in excellent agreement with the Pu(IV) reference spectrum reported by Brendebach et al. (2009). XANES spectra of Pu solid phases in the presence of ISA and Ca(II) are also virtually the same as the XANES spectrum of PuO_2(ncr,hyd) "Pu starting material" reported in (Tasi et al., 2018b).

3.1.4.3. EXAFS. The k^2-weighted EXAFS data shown in Fig. 6 for Pu solid phases recovered from solubility experiments in HQ- and Sn(II)-systems (top row: Fourier-transform magnitude, imaginary part and fit results in R-space, bottom row: raw data, Fourier-filtered data and fit results in k-space) are perfectly in agreement with our previous results obtained in the absence of Ca(II) (Tasi et al., 2018a). The corresponding metric parameters are listed in Table 1. The fit results obtained for both Pu phases are identical within the error margins and very similar to those obtained for the "Pu starting material" as discussed previously (Tasi et al., 2018b). This observation corroborates our *in-situ* XRD and XANES results: the initial PuO_2(ncr,hyd) starting material remains stable in the presence of ISA and Ca(II) and is the solid phase controlling the solubility of Pu in these systems. Note that the results

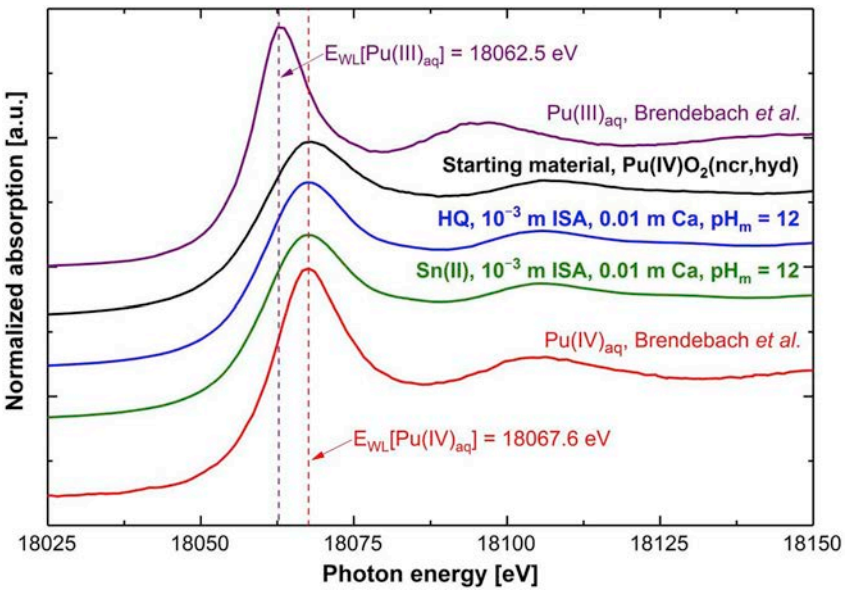

Fig. 5. Pu L_{III}–edge XANES spectra of solid phases recovered from HQ- (blue lines) and Sn(II)-buffered (green lines) systems equilibrated in solutions with $m(ISA)_{tot} = 10^{-3}$ m, $m(Ca)_{tot} = 10^{-2}$ m and $pH_m = 12$ ($t_{eq} = 150$ days). The spectra of the references for the aqueous species of Pu(III) (purple line, position of WL = 18062.5 eV) and Pu(IV) (red line, position of WL = 18067.6 eV) reported in Brendebach et al. (2009) and the spectra of the PuO_2(ncr,hyd) "Pu starting material" reported in Tasi et al. (2018b) are shown for comparison. (For interpretation of the references to colour in this figure legend, the reader is referred to the Web version of this article.)

obtained by EXAFS indicate the presence of significant local disorder and deviations from the ideal PuO_2 fluorite-type crystal structure, which are not visible in the XRD pattern.

3.2. Thermodynamic description of the system Ca(II)–Pu–OH–ISA

Solid phase characterization summarized in Section 3.1.4 confirms PuO_2(ncr,hyd) as solid phase controlling the solubility of Pu in the investigated systems at $pH_m = 12$. Based on the results obtained for analogous Pu–ISA systems in the absence of Ca(II) (see Tasi et al., 2018a), we can safely argue that PuO_2(ncr,hyd) is also the solid phase controlling the solubility of Pu under less alkaline conditions. A separate discussion on the solubility of Pu at $pH_m = 12.4$ is provided in Section 3.2.1. Chemical reactions according to Equations (1) and (4)) are expected to define the baseline of Pu solubility under alkaline, reducing conditions in the absence of ISA and Ca(II). Equations (2–3) and (5–6) were used in combination with equilibrium constants and SIT ion interaction coefficients summarized in Table A1 and Table A2 of the

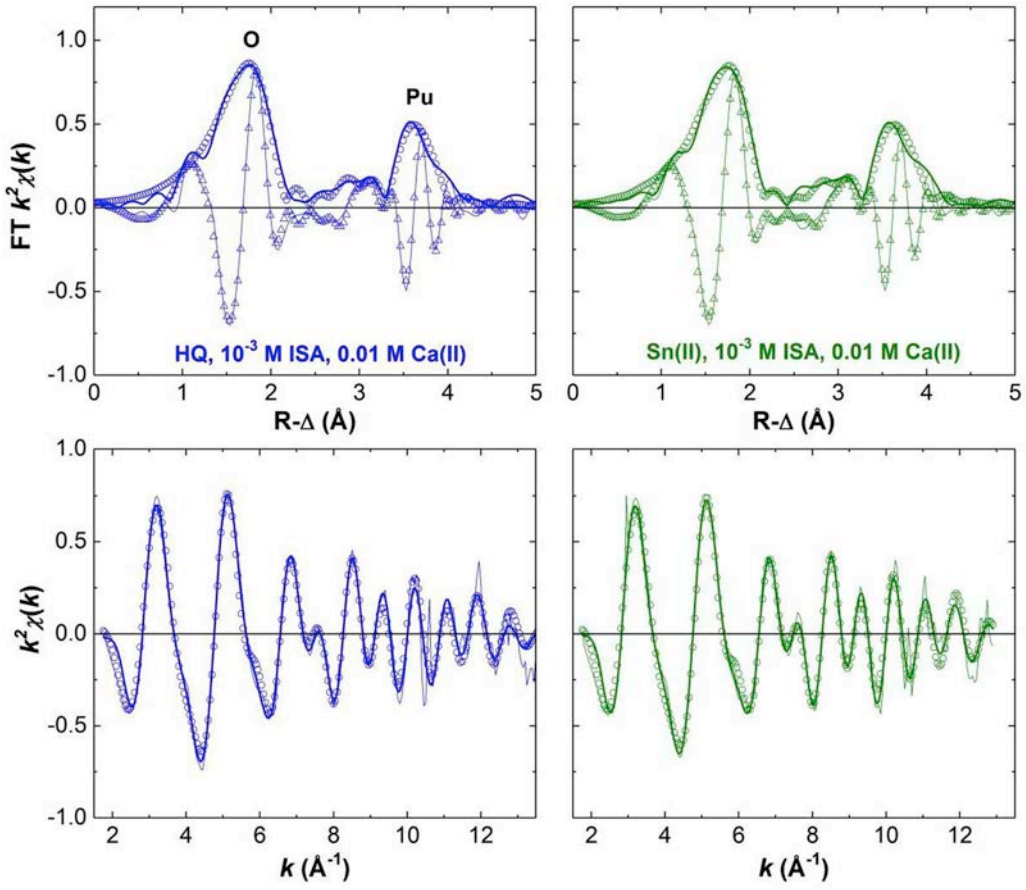

Fig. 6. Pu L_{III}–edge EXAFS fit results for solid phases recovered from HQ- (left pannel) and Sn(II)-buffered (right pannel) solution equilibrated with $m(ISA)_{tot} = 10^{-3}$ m, $m(Ca)_{tot} = 10^{-2}$ m and $pH_m = 12$ ($t_{eq} = 150$ days) – top row: FT magnitude (solid line), fit magnitude (open circles), FT real part (thin solid line) and fit real part (open triangles); bottom row: Fourier-filtered data (solid line), raw data (thin solid line), back-transformed fit (open circles).

Table 1
Data range and metric parameters extracted by least-squares fitting of EXAFS data shown in Fig. 6.

Sample	k-range (Å^{-1})	shell	N	R (Å)	ΔE_0 (eV)[a]	σ^2 (Å^2)	r-factor (%)
	fit-range (Å)						
HQ	1.75–13.58	O	6.2	2.28	−2.19	0.0086	3.1
	0.92–4.11	Pu	4.6	3.78		0.0047	
Sn(II)	1.75–12.92	O	6.0	2.29	−1.90	0.0085	2.9
	0.92–4.11	Pu	4.3	3.78		0.0039	

$S_0^2 = 1.0$ fixed (slightly underestimating N in all fits).
Errors: $R_{Pu\text{-}O}$ 0.01 Å, $R_{Pu\text{-}Pu}$ 0.02 Å
[a] Global parameter for both shells.

Appendix to calculate the corresponding solubility curves of PuO_2(ncr,hyd) shown in Figs. 1–3. Redox conditions initially required in the redox equilibrium for the Sn(II)-buffered system (within Equation (4)) were set to (pe + pHm) = 1.5 as determined experimentally in this work.

$$Pu(IV)O_2(am,hyd) + n\ H^+ \Leftrightarrow Pu(IV)(OH)_{4-n}^{n+} + (n-2)\ H_2O(l) \quad (1)$$

$$\log {}^*K^\circ_{IVs,(4-n)} = \log {}^*K'_{IVs,(4-n)} + \log \gamma_{Pu(IV)(OH)4-n}{}^{n+} + (n-2)\log a_w - n \log \gamma_H{}^+ \quad (2)$$

$$\log {}^*K'_{IVs,(4-n)} = \log m_{Pu(IV)(OH)4-n}{}^{n+} + n\ pH_m \quad (3)$$

$$Pu(IV)O_2(am,hyd) + (1+n)\ H^+ + e^- \Leftrightarrow Pu(III)(OH)_{3-n}^{n+} + (n-1)\ H_2O(l) \quad (4)$$

$$\log {}^*K^\circ_{IVs/III,(3-n)} = \log {}^*K'_{IVs/III,(3-n)} + \log \gamma_{Pu(III)(OH)3-n}{}^{n+} + pe + (n-1)\log a_w - (1+n)\log \gamma_H{}^+ \quad (5)$$

$$\log {}^*K'_{IVs/III,(3-n)} = \log m_{Pu(III)(OH)3-n}{}^{n+} + (1+n)\ pH_m \quad (6)$$

In the presence of ISA and absence of Ca(II), the formation of ternary complexes Pu(III)/Pu(IV)–OH–ISA add further dissolved Pu species to the "solubility baseline" defined by $Pu(III)(OH)_{3-n}^{n+}$ and $Pu(IV)(OH)_{4-n}^{n+}$ hydrolysis species. Based upon the thermodynamic model derived in Tasi et al. (2018a), equilibrium reactions according to Equations (7) and (10)) define the formation of the aqueous species $Pu(IV)(OH)_3ISA_{-yH}^{-y}$ (with y = 1 or 2) and $Pu(III)(OH)ISA_{-H}$(aq) in equilibrium with PuO_2(ncr,hyd). Equations ((2), (3), (5), (6), (8) and (9)) and 11 – 12 were used in combination with equilibrium constants and SIT ion interaction coefficients summarized in Table A1 and Table A2 of the Appendix to calculate the solubility of PuO_2(ncr,hyd) in the presence of ISA and absence of Ca(II) shown in Figs. 1–3 and Fig. 7.

$$Pu^{4+}(aq) + ISA^- + 3\ H_2O(l) \Leftrightarrow Pu(IV)(OH)_3ISA_{-yH}^{-y} + (3+y)\ H^+ \quad (7)$$

$$\log {}^*\beta^\circ_{1,3+y,1} = \log {}^*\beta'_{1,3+y,1} + \log \gamma_{Pu(IV)(OH)3ISA-yH}{}^{-y} + (3+y)\log \gamma_H{}^+ - \log \gamma_{Pu(aq)}^{4+} - \log \gamma_{ISA}{}^- - 3\log a_w \quad (8)$$

$$\log {}^*\beta^\circ_{1,3+y,1} = \log a_{Pu(IV)(OH)3ISA-yH}{}^{-y} + (3+y)\log a_H{}^+ - \log a_{Pu(aq)}^{4+} - \log a_{ISA}{}^- \quad (9)$$

$$Pu^{3+}(aq) + ISA^- + H_2O(l) \Leftrightarrow Pu(III)(OH)ISA_{-H}(aq) + 2\ H^+ \quad (10)$$

$$\log {}^*\beta^\circ_{1,2,1} = {}^*\beta'_{1,2,1} + \log \gamma_{Pu(III)(OH)ISA-H(aq)} + 2\log \gamma_H{}^+ - \log a_{Pu(aq)}^{3+} - \log \gamma_{ISA}{}^- - \log a_w \quad (11)$$

$$\log {}^*\beta^\circ_{1,2,1} = \log a_{Pu(III)(OH)ISA-H(aq)} + 2\log a_H{}^+ - \log a_{Pu(aq)}^{3+} - \log a_{ISA}{}^- \quad (12)$$

3.2.1. Chemical and thermodynamic model for the system Ca(II)-Pu(IV)-OH-ISA

Based on the solid phase characterization and slope analysis of the solubility data summarized in Section 3.1, chemical reactions according to Equations (13) and (14) are proposed to control the solubility of Pu (IV) in alkaline HQ-systems in the presence of ISA and Ca(II).

$$Pu(IV)O_2(ncr,hyd) + ISA^- + Ca^{2+} + 2\ H_2O(l) \Leftrightarrow Ca(II)Pu(IV)(OH)_4ISA^+ \quad (13)$$

$$Pu(IV)O_2(ncr,hyd) + ISA^- + Ca^{2+} + 3\ H_2O(l) \Leftrightarrow Ca(II)Pu(IV)(OH)_5ISA(aq) + H^+ \quad (14)$$

The species $Ca(II)Pu(OH)_4ISA^+$ dominates the aqueous speciation of Pu within $8 \le pH_m \le 11$, whereas $Ca(II)Pu(OH)_5ISA(aq)$ becomes predominant at $pH_m > 11$. Although the predominance of a positively charged species of Pu may seem unlikely in alkaline media, it basically reflects the interaction of the species prevailing in solution within this pH_m-region: $Pu(OH)_4ISA^-$ (see Tasi et al., 2018a) and Ca^{2+}. Note also that the proposed stoichiometries for the Ca(II)–Pu(IV)–OH–ISA complexes formally assume highly hydrolysed moieties ("$Pu(OH)_4$" and "$Pu(OH)_5^-$") within the quaternary complex species, where only the carboxylic group of ISA is deprotonated. However, protons released in the complexation reaction can also be assigned to deprotonations of alcohol groups of ISA. The structures of the complexes forming are further discussed in section 3.3 on the basis of DFT calculations performed in the present study.

Two relevant aspects must be accounted for with regard to the chemical model defined by the equilibrium reactions according to Equations (13) and (14):

i. The proposed chemical model is based on solubility data at $pH_m \le 12$. Above this pH_m, other phenomena not yet understood affect solubility, decreasing (or limiting) $m(Pu)_{tot}$ in solution. The use of this chemical model (and the accordingly derived thermodynamic model) beyond this pH_m value will overestimate solubility data, (providing a "conservative" upper limit).
ii. Solubility experiments with varying $m(ISA)_{tot}$ and $m(Ca)_{tot}$ were only conducted at $pH_m = 12$. Consequently, the stoichiometries Pu:ISA and Pu:Ca in reaction (13) are based on the assumption that the same stoichiometry of the Pu(IV)–OH–ISA complex in the absence of Ca(II) is retained, and that only one Ca^{2+} ion is attached to this structure. The complexation of a second Ca^{2+} ion to the Ca(II) $Pu(IV)(OH)_4ISA^+$ moiety seems unlikely for evident electrostatic reasons.

Although the favoured chemical model involves the formation of the two species 1:1:4:1 ($Ca(II)Pu(IV)(OH)_4ISA^+$) and 1:1:5:1 ($Ca(II)Pu(IV)(OH)_5ISA(aq)$), a number of additional stoichiometries (1:1:6:1, 1:1:5:2, 2:1:5:1, 2:1:5:2 and 2:1:6:2) were tested as alternative to the complex 1:1:5:1 in the modelling of the solubility data. We note that previous investigations on the system Ca(II)–Th(IV)–OH–ISA (Vercammen et al., 2001; Tits et al., 2005) proposed the predominance of complexes with a stoichiometry Th(IV):ISA 1:2. This possibility is also accounted for in three of the alternative stoichiometries considered (1:1:5:2, 2:1:5:2 and 2:1:6:2). Due to the limited experimental data available at $pH_m \le 11$ (*e.g.* only data at $m(ISA)_{tot}$ = constant and $m(Ca)_{tot}$ = constant), the evaluation of alternative stoichiometries to the complex 1:1:4:1 ($Ca(II)Pu(IV)(OH)_4ISA^+$) was disregarded in the modelling of the solubility data.

General equilibrium constants (at the reference state, $I \rightarrow 0$) for the formation of the two quaternary complexes proposed in this work, $Ca(II)_zPu(IV)(OH)_{4+y}(ISA)_x^{(2z-x-y)}$, can be expressed from Equations (15) and (16):

$$Pu^{4+}(aq) + x\ ISA^- + (4+y)\ H_2O(l) + z\ Ca^{2+}(aq) \Leftrightarrow Ca(II)_zPu(IV)(OH)_{4+y}(ISA)_x^{2z-x-y} + (4+y)\ H^+ \quad (15)$$

$$\log {}^*\beta^\circ_{z,1,4+y,x} = \log a_{Ca(II)zPu(IV)(OH)4+y(ISA)x}{}^{2z-x-y} + (4+y)\log a_H{}^+ - \log a_{Pu(aq)}^{4+} - x\log a_{ISA}{}^- - z\log a_{Ca}{}^{2+} \quad (16)$$

Considering equilibrium reactions according to Equations ((1), (4),

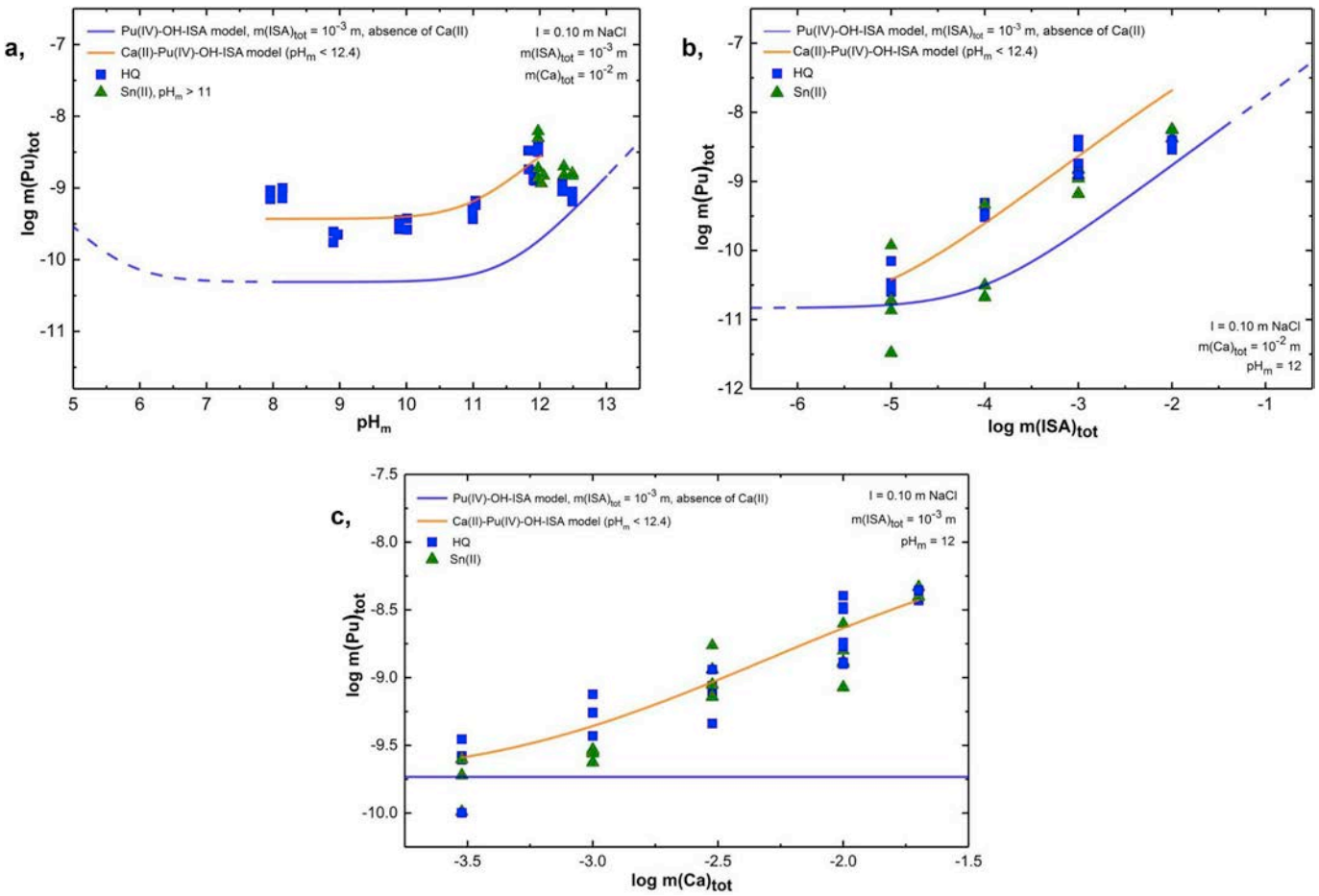

Fig. 7. Experimentally measured $m(Pu)_{tot}$ in equilibrium with PuO_2(ncr,hyd) in HQ- (■) and Sn(II)-buffered (▲, $pH_m > 11$) systems as function of pH_m (a), log m $(ISA)_{tot}$ (b) and log $m(Ca)_{tot}$ (c). Solubility lines in orange are calculated with the chemical and thermodynamic models derived in this work for the quaternary system Ca(II)–Pu(IV)–OH–ISA. Blue lines (solid and dashed) correspond to the solubility of PuO_2(ncr,hyd) calculated using the chemical and thermodynamic models derived in our previous work for the ternary system Pu(IV)–OH–ISA (Tasi et al., 2018a). (For interpretation of the references to colour in this figure legend, the reader is referred to the Web version of this article.)

(7), (10) and (16), the total concentration of Pu in solution can be calculated in Equation (17). Note that $m_{Ca^{2+}}$ and m_{ISA^-} are calculated considering the formation of binary Ca(II)–OH and ternary Ca(II)–O-H–ISA complexes using thermodynamic data summarized in Tables A2 and A3 in the Appendix.

$$m(Pu)_{tot}^{calc,n} = \Sigma_{n=1}^{4}({}^{*}K'_{IVs,(4-n)}\ (m_{H^+})^n) + {}^{*}K'_{IVs,0}[({}^{*}\beta'_{1,4,1}\ (m_{ISA^-}) + {}^{*}\beta'_{1,5,1}\ (m_{ISA^-})\ (m_{H^+})^{-1})] + {}^{*}K'_{IVs,0}[\Sigma_{i=1}^{2}\ ({}^{*}\beta'_{zi,1,\ 4+yi,xi}(m_{ISA^-})_i^x\ (m_{H^+})_i^{-y}\ (m_{Ca^{2+}})_i^z)] + {}^{*}K'_{IVs,4,1,8}\ (m_{H^+})^{-4}\ (m_{Ca^{2+}})^4 \quad (17)$$

For all evaluated chemical models, the values of the equilibrium constants ${}^{*}\beta^{\circ}_{1,1,4,1}$ and ${}^{*}\beta^{\circ}_{z,1,4+y,x}$ were optimized to obtain the best fit of the solubility data set. The optimization targeted the minimization of the square root of the averaged sum of squared residuals for measured and calculated $m(Pu)_{tot}$, with the objective function f_{obj} $({}^{*}\beta^{\circ}_{z,1,4+y,x})$. The minimization was performed using the PHREEPLOT – PHREEQC software packages (see Tasi et al. (2018a) for a detailed description of the method). The first step of the fitting process involved the optimization of the stoichiometry of complex 2, and (because of the large number of stoichiometries/species evaluated) the effect of ionic strength was calculated using only the Debye–Hückel term of the SIT formulism. In a second step, after completing the optimization of the stoichiometry of complex 2, an additional fitting exercise was performed considering the complete SIT formulism in the optimization of the corresponding equilibrium constants.

Table 2 shows values of the R^2 parameter and the objective function f_{obj} $({}^{*}\beta^{\circ}_{z,1,4+y,x})$ resulting from the fitting procedures using the different chemical models discussed above. Chemical models involving the formation of (1:1:4:1 + 1:1:5:1) or (1:1:4:1 + 1:1:6:1) complexes give an almost identical statistical representation of the experimental data. However, the first option is favoured in this work for the sake of simplicity and to retain a closer consistency with the chemical model reported for the ternary system Pu(IV)–OH–ISA (Tasi et al., 2018a). Table 2 also demonstrates that those stoichiometries considering the participation of two ISA molecules result in significantly worse values for R^2 and f_{obj} parameters. In contrast to previous observations reported for Th(IV) (Vercammen et al., 2001; Tits et al., 2005), these results provide conclusive evidence that only one ISA molecule participates in the formation of a quaternary complex with Pu(IV) and Ca(II).

Table 2
Quality parameters obtained in the optimization of the stoichiometry of the quaternary Ca(II)–Pu(IV)–OH–ISA complexes.

	Ca (z): Pu(IV): OH (4 + y): ISA (x) ratios					
1st complex	**1:1:4:1**	1:1:4:1	1:1:4:1	1:1:4:1	1:1:4:1	1:1:4:1
2nd complex	**1:1:5:1**	*1:1:6:1*	*1:1:5:2*	*2:1:5:1*	*2:1:5:2*	*2:1:6:2*
R^2 (%)	**73.14**	73.26	39.46	69.35	39.46	39.46
$f_{obj}({}^{*}\beta'_{z,1,4+y,x})$	**0.273**	0.273	0.410	0.293	0.410	0.410

Based on the selected stoichiometries (1:1:4:1 and 1:1:5:1), equilibrium constants ${}^{*}\beta^{\circ}_{1,1,4,1}$ and ${}^{*}\beta^{\circ}_{1,1,5,1}$ were optimized to obtain the lowest residuals between the calculated (Equation (17)) and experimentally measured $m(Pu)_{tot}$. The SIT formalism as described in

Equation (18) was used to account for the effect of ionic strength on the equilibrium constants of the related complexes Ca(II)Pu(IV)$(OH)_4ISA^+$ (y = 0 in Equation (18)) and Ca(II)Pu(IV)$(OH)_5ISA$(aq) (y = 1 in Equation (18)). A SIT ion interaction coefficient for the complex Ca(II)Pu(IV)$(OH)_4ISA^+$ with Cl^- was estimated as ε(Ca(II)Pu(IV)$(OH)_4ISA^+$, Cl^-) = –(0.05 ± 0.10) kg·mol^{-1} following the charge analogy described in the work of Hummel (2009). The ion interaction coefficient of the neutral complex Ca(II)Pu(IV)$(OH)_5$ISA(aq) is zero by definition in SIT.

$$\log {}^{*}\beta^{\circ}_{1,1,4+y,1} = \log {}^{*}\beta'_{1,1,4+y,1} + \log \gamma_{CaPu(IV)(OH)4+yISA}{}^{1-y} + (4 + y) \log \gamma_{H}{}^{+} - \log \gamma_{Pu(aq)}^{4+} - \log \gamma_{ISA}{}^{-} - \log \gamma_{Ca(aq)}^{2+} - (4 + y) \log a_w \quad (18)$$

The optimization of log ${}^{*}\beta^{\circ}_{1,1,4,1}$ and log ${}^{*}\beta^{\circ}_{1,1,5,1}$ resulted in:

$$\log {}^{*}\beta^{\circ}_{1,1,4,1}(Ca(II)Pu(IV)(OH)_4ISA^+) = -(1.66 \pm 0.10) \quad (19)$$

$$\log {}^{*}\beta^{\circ}_{1,1,5,1}(Ca(II)Pu(IV)(OH)_5ISA(aq)) = -(12.70 \pm 0.08) \quad (20)$$

The stability of the complexes Ca(II)Pu(IV)$(OH)_4ISA^+$ and Ca(II)Pu(IV)$(OH)_5$ISA(aq) can be better assessed by defining the step-wise reactions from the corresponding ternary complexes (Pu(IV)$(OH)_3ISA_{-H}{}^-$ and Pu(IV)$(OH)_3ISA_{-2H}{}^{2-}$) and Ca^{2+}:

$$Pu(IV)(OH)_4ISA^- + Ca^{2+} \Leftrightarrow CaPu(IV)(OH)_4ISA^+ \quad (21)$$

$$Pu(IV)(OH)_5ISA^{2-} + Ca^{2+} \Leftrightarrow CaPu(IV)(OH)_5ISA(aq) \quad (22)$$

with:

$$\log {}^{*}K^{\circ}_{1,1,4,1} = \log {}^{*}\beta^{\circ}_{1,1,4,1} - \log {}^{*}\beta^{\circ}_{1,4,1} = (3.37 \pm 0.16) \quad (23)$$

$$\log {}^{*}K^{\circ}_{1,1,5,1} = \log {}^{*}\beta^{\circ}_{1,1,5,1} - \log {}^{*}\beta^{\circ}_{1,5,1} = (4.22 \pm 0.15), \quad (24)$$

where log ${}^{*}\beta^{\circ}_{1,4,1}$ and log ${}^{*}\beta^{\circ}_{1,5,1}$ are the formation constants for the ternary complexes Pu(IV)$(OH)_4ISA^-$ and Pu(IV)$(OH)_5ISA^{2-}$ as determined in Tasi et al. (2018a). The values of log ${}^{*}K^{\circ}_{1,1,4,1}$ and log ${}^{*}K^{\circ}_{1,1,5,1}$ indicate that the quaternary complexes CaPu(IV)$(OH)_4ISA^+$ and CaPu(IV)$(OH)_5$ISA(aq) are moderately strong, and that (as expected according to their charges) Ca^{2+} reacts stronger with Pu(IV)$(OH)_5ISA^{2-}$ than with Pu(IV)$(OH)_4ISA^-$.

Fig. 7 shows the experimental solubility data collected in HQ-buffered systems, and the corresponding solubility curves calculated using the chemical and thermodynamic models derived in this work for the system Ca(II)–Pu(IV)–OH–ISA. Although not considered in the development of the thermodynamic model, Fig. 7 includes also experimental solubility data obtained in Sn(II)-buffered systems at pH_m > 11. For comparison, the figures also show the solubility of PuO_2(ncr,hyd) considering only the formation of ternary complexes Pu(IV)–OH–ISA and using chemical and thermodynamic models reported in Tasi et al. (2018a).

Fig. 7 shows that the chemical and thermodynamic models derived in this work describe well most of the experimental solubility data. However, relatively large deviations (0.5 – 1 $\log_{10}$-units) are observed at pH_m > 12 and $m(ISA)_{tot} \geq 0.01$ m). As discussed in Section 3.1.1, these observations likely hint to the formation of yet undefined Ca(II)–Pu(IV)–OH–ISA(s) solid phase(s). We note further that the thermodynamic model derived under mildly reducing conditions (HQ-systems) provides also reasonable predictions for the solubility of Pu under strongly reducing conditions (Sn(II)-systems) at pH_m > 11.

3.3. DFT calculations on the complexes Ca(II)Pu(IV)$(OH)_4ISA^+$ and Ca(II)Pu(IV)$(OH)_5$ISA(aq)

DFT calculations summarized in this section provide detailed information on the structure of the quaternary complexes Ca(II)–Pu(IV)–OH–ISA, with focus on assessing the hydrolysis of Pu^{4+} *vs.* the deprotonation of OH-groups of the ISA molecule in the presence of Ca(II) ions. These calculations follow the same strategy outlined in our first contribution (Tasi et al., 2018a). Whilst keeping the charge of the complex constant, several configurations involving different number of hydroxide ions (OH^-) and deprotonated alcohol groups of ISA (-C-O^-) were tested. Besides for Pu(IV), the possible coordination of OH^- ions to Ca(II) was also evaluated in the calculations:

(i) Ca(II)$(OH)_z$Pu(IV)$(OH)_x$ISA$_{-yH}(H_2O)_{8-z}$(aq) (x + y + z = 5);
(ii) Ca(II)$(OH)_z$Pu(IV)$(OH)_x$ISA$_{-yH}(H_2O)_{8-z}{}^+$ (x + y + z = 4),

where ISA_{-yH} corresponds to an ISA molecule with *y* deprotonated alcohol groups and a charge of –(y+1). In each case, several starting geometries were probed both with and without the approximation of the aqueous solution phases with COSMO to confirm that a reasonable local minimum was found for the calculated structures.

3.3.1. Ca(II)$(OH)_z$Pu(IV)$(OH)_x$ISA$_{-yH}(H_2O)_{8-z}$(aq) (x + y + z = 5)

For the complexes Ca(II)$(OH)_z$Pu(IV)$(OH)_x$ISA$_{-yH}(H_2O)_{8-z}$(aq) (x + y + z = 5), we found the energetically lowest and hence most favourable structures with and without COSMO with the α-OH of ISA (second carbon: ISA (C_2) adjacent to the carboxylate group) and the alcohol group of the fourth carbon atom (δ-OH) deprotonated (labelled as ISA (C_4)). Almost in the same way as without Ca(II), the interaction of ISA with Pu(IV) involves two deprotonated alcohol groups and the carboxylate group. Three hydroxide ions and three water molecules remain in the first coordination shell of the Pu(IV) ion, and six water molecules in the first coordination shell of Ca(II). The resulting structure as optimized by DFT can be described as Ca(II)Pu(IV)$(OH)_3ISA_{-2H}(H_2O)_8$(aq) (see Fig. 8).

Atomic distances calculated by DFT and DFT + COSMO for the optimized structures of Ca(II)Pu(IV)$(OH)_3ISA_{-2H}(H_2O)_8$(aq) are summarized in Table 3. Shorter distances are found for Pu(IV)-ISA (-C_4-O^-) (232/235 pm), Pu(IV)-OH^-(233-245/233-242 pm) and Pu(IV)–ISA (-C_2-O^-) (235/236 pm) compared to the longer distances calculated for Pu

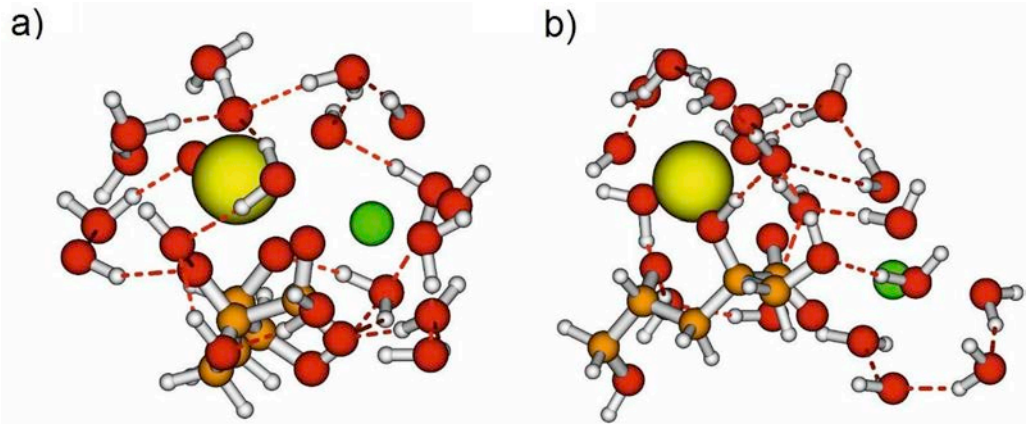

Fig. 8. Structures of the complexes a) Ca(II)Pu(IV)$(OH)_3ISA_{-2H}(H_2O)_8$(aq) and b) Ca(II)Pu(IV)$(OH)_3ISA_{-H}(H_2O)_8{}^+$ as optimized in this work by DFT calculations. Pu: yellow, Ca: green, oxygen: red, carbon: orange, hydrogen: grey. (For interpretation of the references to colour in this figure legend, the reader is referred to the Web version of this article.)

Table 3
Pu(IV)-O and Ca(II)-O distances (in pm) calculated by DFT and DFT + COSMO for the $Ca(II)Pu(IV)(OH)_3ISA_{-2H}(H_2O)_8(aq)$ and $Ca(II)Pu(IV)(OH)_3ISA_{-H}(H_2O)_8^{+}$ complexes as optimized in this work.

$Ca(II)Pu(IV)(OH)_3ISA_{-2H}(H_2O)_8(aq)$

bond	DFT	+COSMO	bond	DFT	+COSMO
Pu(IV)-ISA (-C_4-O^-)	232	235	Pu(IV)-ISA (-C_2-O^-)	235	236
Pu(IV)-OH^-	233	233	Pu(IV)-ISA (-COO^-)	255	258
Pu(IV)-OH^-	234	233	Pu(IV)-OH_2	245	248
Pu(IV)-OH^-	245	242	Pu(IV)-OH_2	273	265
Pu(IV)-Ca(II)	464	466			
Ca(II)-OH_2	239–254	237–257	Ca(II)- ISA (-COO^-)	246	248

$Ca(II)Pu(IV)(OH)_3ISA_{-H}(H_2O)_8^{+}$

bond	DFT	+COSMO	bond	DFT	+COSMO
Pu(IV)-ISA (-C_4-O^-)	230	230	Pu(IV)-ISA (-COO^-)	239	246
Pu(IV)-OH^-	229	228	Pu(IV)-ISA (-C_2-OH)	251	253
Pu(IV)-OH^-	230	232	Pu(IV)-OH_2	256	255
Pu(IV)-OH^-	240	237	Pu(IV)-OH_2	262	259
Pu(IV)-Ca(II)	546	496			
Ca(II)-OH_2	231–271	235–262	Ca(II)- ISA (-COO^-)	240	248,262

(IV)–ISA (-COO^-) (255/258 pm) and Pu(IV)–H_2O (259 pm/259 pm). In both calculations, the distances Pu(IV)-Ca(II) are similar (464/466 pm), the Ca(II)- ISA (-COO^-) (246/248 pm) and the Ca(II)-OH_2 distances vary from 239 to 254 and 237–257 pm, respectively. Both are slightly shorter compared to the corresponding Pu(IV) distances.

3.3.2. $Ca(II)(OH)_zPu(IV)(OH)_xISA_{-yH}(H_2O)_{8-z}^{+}$ (x + y + z = 4)

For this series of complexes, we identified $Ca(II)Pu(IV)(OH)_3ISA_{-H}(H_2O)_8^{+}$ (with a deprotonated alcohol group on ISA (C_4)) as the energetically lowest and hence most favourable structure. However, two other configurations were found to be energetically very close to the structure: $Ca(II)Pu(IV)(OH)_2ISA_{-2H}(H_2O)_8^{+}$ and $Ca(II)Pu(IV)(OH)_3ISA_{-H}(H_2O)_8^{+}$ (both, with the ISA (C_2) deprotonated). These structures hold electronic energies only 2 kJ/mol and 8 kJ/mol, respectively, above the lowest lying configuration. Since these differences are very small we additionally determined the thermodynamical solvent contributions by means of COSMO model, but this did not change the result. $Ca(II)Pu(IV)(OH)_3ISA_{-H}(H_2O)_8^{+}$ remains the complex with the lowest energy and the other two complexes possess energies 8 and 15 kJ/mol higher, respectively.

In the $Ca(II)Pu(IV)(OH)_3ISA_{-H}(H_2O)_8^{+}$ complex, Pu(IV)-ISA (-C_4-O^-) (230/230 pm), Pu(IV)-OH^-(229-240/228-237 pm) distances are the shortest. Due to the structural changes following the different deprotonation schemes, Pu(IV)-ISA (-COO^-) (239/246 pm) is shorter compared to Pu(IV)-ISA (-C_2-OH) (251/253 pm) and the Pu(IV)-OH_2 (256, 262/255, 259 pm) are longest. The Pu(IV)-Ca(II) (546/496 pm) distances are much longer compared to the $Ca(II)Pu(IV)(OH)_3ISA_{-2H}(H_2O)_8(aq)$ case due to the higher positive charge of the complex. The Ca(II)- ISA (-COO^-) (240/248, 262 pm) and the Ca(II)-OH_2 distances vary from 231 to 271 and 235–262 pm, respectively.

3.4. Comparison of the thermodynamic model derived in this work with data available in the literature

Table 4 summarizes the equilibrium constants derived in the present work for the formation of Ca(II)–Pu(IV)–ISA–OH complexes prevailing under reducing, alkaline to hyperalkaline conditions in the presence of ISA and Ca(II). Table 5 lists SIT ion interaction coefficients considered in the present work for the newly identified species. Although the stoichiometry of the quaternary Ca(II)–Pu(IV)–OH–ISA complexes is the same as defined in Section 3.2, information gained by DFT calculations as described in Section 3.3 are considered for the definition of the chemical structure of these complexes. This involves the deprotonation of one ($Ca(II)Pu(IV)(OH)_3ISA_{-H}^{+}$) and two ($Ca(II)Pu(IV)(OH)_3ISA_{-2H}(aq)$) alcohol groups of ISA.

Table 4
Chemical equilibria and related equilibrium constants (at $I \rightarrow 0$ m) derived in the present study for the Ca(II)–Pu(IV)–OH–ISA system.

Chemical equilibria	log $*\beta^{\circ}_{(1,1,4+y,1)}$
$Pu^{4+} + ISA^- + 3\,H_2O(l) + Ca^{2+} \Leftrightarrow Ca(II)Pu(IV)(OH)_3ISA_{-H}^{+} + 4\,H^+$	–(1.66 ± 0.10)
$Pu^{4+} + ISA^- + 3\,H_2O(l) + Ca^{2+} \Leftrightarrow Ca(II)Pu(IV)(OH)_3ISA_{-2H}(aq) + 5\,H^+$	–(12.70 ± 0.08)

Table 5
SIT ion interaction coefficients considered in the present study for the quaternary complexes Ca(II)–Pu(IV)–ISA–OH.

species i	species j	ε(i,j) [kg·mol^{-1}]
$Ca(II)Pu(IV)(OH)_3ISA^{+}$	Cl^-	–(0.05 ± 0.10)[a]
$Ca(II)Pu(IV)(OH)_3ISA^{-2H}(aq)$	Cl^-/Na^+	0.00[b]

[a] Estimated values based on the work of Hummel (2009).
[b] Defined to be zero by definition within SIT formalism.

Chemical and thermodynamic models derived in this work for the system Ca(II)–Pu(IV)–OH–ISA can be compared with analogous thermodynamic data reported for the system Ca(II)–Th(IV)–OH–ISA by Vercammen et al. (2001), Tits et al. (2002) and Tits et al. (2005) (see Introduction for detailed discussion of these publications). Fig. 9 shows the predominance diagrams of Pu(IV) and Th(IV) calculated for pH_m = constant = 9 and 12, with $-6 \leq \log m(ISA)_{tot} \leq -1$ and $-4 \leq \log m(Ca)_{tot} \leq -1.5$.

Fig. 9a–d shows very different aqueous speciation schemes for Th(IV) and Pu(IV) in the presence of ISA and Ca(II). The predominance of complexes with An(IV):ISA ratios of 1:1 for Pu(IV) and 1:2 for Th(IV) might be considered consistent with the observations available for the ternary systems in the absence of Ca(II) (see discussion in Tasi et al. (2018a)). To some extent, differences in the stoichiometry of the quaternary complexes described for Th(IV) (with the structure of $Ca(II)Th(IV)(OH)_4ISA_2(aq)$) and Pu(IV) (with $Ca(II)Pu(IV)(OH)_4ISA^{+}$ and $Ca(II)Pu(IV)(OH)_5ISA^-$) can be justified on the basis of the larger size of Th^{4+} (r = 1.08 ± 0.02 Å) compared to Pu^{4+} (r = 1.01 ± 0.02 Å), which induces also a stronger hydrolysis for Pu(IV). However, in our view, the greater stability reported for the quaternary Th(IV) complexes compared to Pu(IV) (see Fig. 9) is not considered to be "real", but rather caused by differences in the experimental method used: Pu(IV): solubility experiments (present work); Th(IV): sorption study, Vercammen et al. (2001), Tits et al. (2002) and Tits et al. (2005). Although our solubility study confirms the role of Ca(II) in stabilizing ternary Pu(IV)–OH–ISA complexes, the "enhanced" stability of the resulting quaternary complexes does not match the predictions based on Th(IV) data. We speculate that the very low concentrations used in the sorption experiments ($1.2{\cdot}10^{-13}$ M ^{234}Th in Vercammen et al. (2001) or 10^{-11} M ^{228}Th in Tits et al. (2005)) might have posed experimental challenges that have been overcome by using larger amounts of Pu(IV) (0.25–1.5 mg ^{242}Pu) as used in our solubility study, but this discussion remains open until additional studies with An(IV) are performed using both methods. The reader is referred to our previous contribution on the ternary system Pu(III/IV)–OH–ISA for further insights on the differences arising between solubility and sorption experiments (Tasi et al., 2018a).

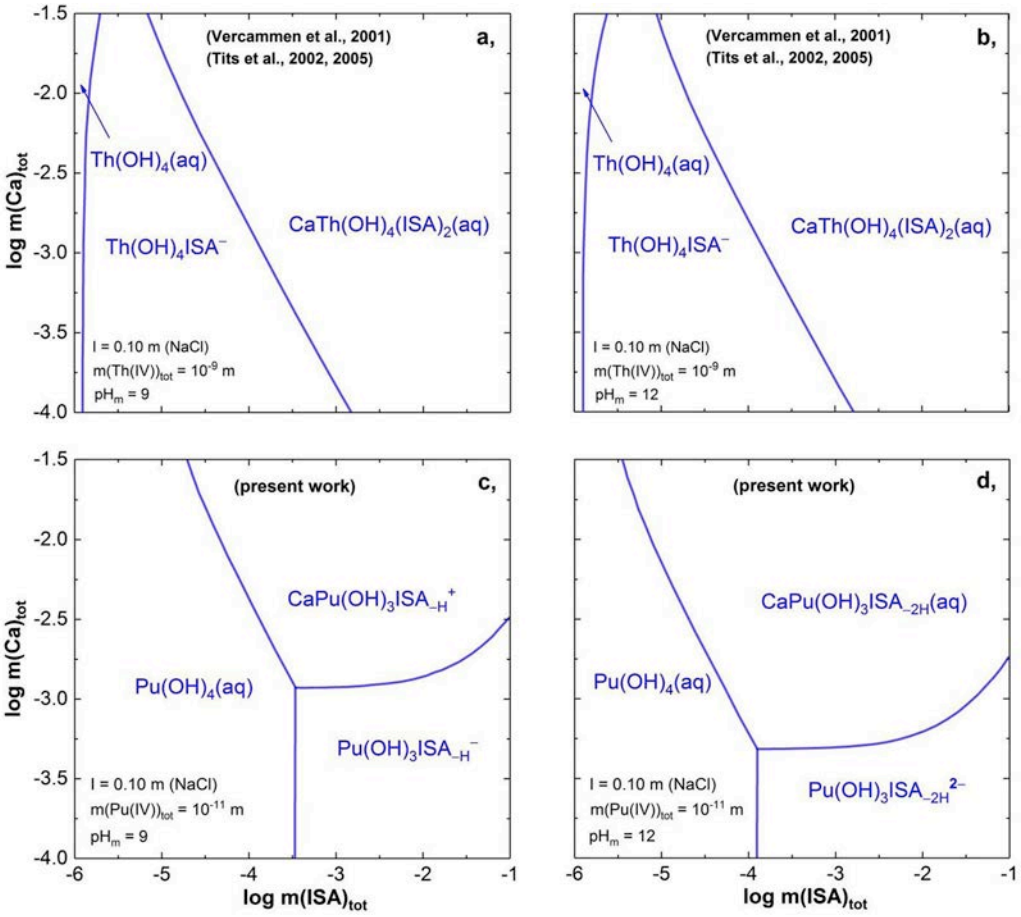

Fig. 9. Predominance diagrams of An (IV) in the presence of ISA ($-6 \leq \log m(ISA)_{tot} \leq -1$) and Ca(II) ($-4 \leq \log m(Ca)_{tot} \leq -1.5$) at I = 0.10 m NaCl. Diagrams calculated for **Th(IV)**: $m(Th(IV))_{tot} = 10^{-9}$ m at **(a)** $pH_m = 9$ and **(b)** $pH_m = 12$, using thermodynamic data reported by Vercammen et al. (2001) and Tits et al. (2002); Tits et al. (2005), and recalculated in Gaona et al. (2008). Diagrams calculated for **Pu (IV)**: $m(Pu(IV))_{tot} = 10^{-11}$ m at **(c)** $pH_m = 9$ and **(d)** $pH_m = 12$, using thermodynamic data derived in the present work.

4. Summary and conclusions

The solubility of Pu in alkaline reducing solutions was systematically investigated in the presence of ISA and Ca(II) within chemical boundary conditions similar to those expected for solutions in contact with cementitious systems.

In-situ XRD, XAFS and analogy with the ternary system Pu–OH–ISA indicate that PuO_2(ncr,hyd) is the solid phase controlling the solubility of Pu in the presence of ISA and Ca(II) at $pH_m \leq 12$. Above this pH_m and at $m(ISA)_{tot} \geq 10^{-2}$ m, the formation of a yet undefined Ca(II)–Pu(IV)–OH–ISA solid phase is suspected to occur. In solutions containing ISA and Ca(II) at $pH_m \leq 12$, the solubility of Pu is significantly enhanced compared to Ca(II)-free systems. This observation strongly supports the formation of quaternary Ca(II)–Pu(IV)–OH–ISA complexes, which was discussed in previous literature for the analogous Th(IV) system. Under mildly reducing conditions ($pe + pH_m \approx 9$), slope analysis of the solubility data ($\log m(Pu)_{tot}$ *vs.* pH_m, $\log m(Pu)_{tot}$ *vs.* $\log m(ISA)_{tot}$ and $\log m(Pu)_{tot}$ *vs.* $\log m(Ca)_{tot}$) in combination with DFT calculations indicates the predominance of the complexes Ca(II)Pu(IV)$(OH)_3ISA_{-H}^{+}$ and Ca(II)Pu(IV)$(OH)_3ISA_{-2H}$(aq) in the aqueous phase. The same speciation scheme explains properly the solubility of Pu under very reducing conditions ($pe + pH_m \approx 1.5$) at $pH_m > 11$, although the predominance of ternary Pu(III)–OH–ISA complexes is hinted below this pH_m. Ca(II) plays a key role in destabilizing Pu-ISA colloids, which were found to importantly enhance Pu(IV) solubility (up to 2 $\log_{10}$-units) in Ca-free systems (Tasi et al., 2018a). Chemical and thermodynamic models derived for the system Ca^{2+}–Pu^{4+}–OH^-–Cl^-–ISA^-–H_2O(l) properly explain most of the experimental evidences, but overestimate solubility by 0.5 – 1 $\log_{10}$-units at $pH_m > 12$ and $m(ISA)_{tot} \geq 10^{-2}$ m. The stoichiometry and stability of the quaternary complexes Ca(II)–Pu(IV)–OH–ISA identified in this work differ from those previously reported for the Th(IV) system (Vercammen et al., 2001; Tits et al., 2005). Although such discrepancies can be partially attributed to differences in the solution chemistry of Pu^{4+} (r = 1.01 ± 0.02 Å) and Th^{4+} (r = 1.08 ± 0.02 Å), we suspect that they are also intrinsically related to the method used to derive thermodynamic data (solubility for Pu(IV) and sorption for Th(IV)). We consider that sorption studies using ultra-trace concentrations of a given radionuclide are possibly more sensitive to artifacts than solubility studies with larger amounts of the same radionuclide, but this discussion would benefit from new experimental studies combining both solubility and sorption experiments.

Acknowledgements

The research leading to this study was funded by SKB, the Swedish Nuclear Fuel and Waste Management Company. We acknowledge the KIT light source for provision of instruments at the INE-Beamline station operated by the Institute for Nuclear Waste Disposal (KIT–INE) and we would like to thank the Institute for Beam Physics and Technology (IBPT) for the operation of the storage ring, the Karlsruhe Research Accelerator (KARA). The received support from Frank Geyer and Annika Kaufmann (KIT–INE) for the (SF–)ICP–MS measurements are further gratefully acknowledged.

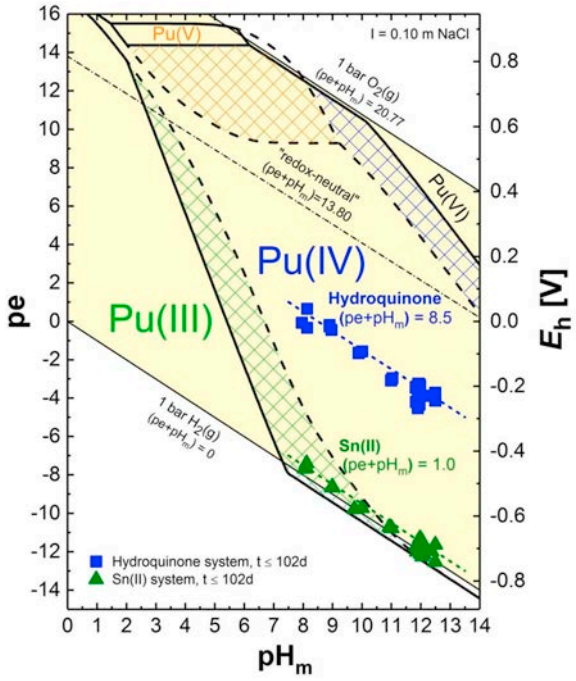

Fig. A1. Pourbaix diagram of Pu calculated for $m_{Pu} = 10^{-5}$ m and $I = 0.1$ m NaCl using thermodynamic and (SIT) activity models as described in the text. pH_m and E_h values experimentally determined for Pu(IV) solubility experiments in the presence of ISA and Ca(II) ions in solution with redox-buffering agents: hydroquinone (■) and Sn(II) (▲). Thick lines correspond to redox borderlines between Pu(IV) and other Pu redox states: solid line is the borderline between Pu solid phases; dashed line is the borderline between Pu aqueous species. Coloured regions indicate equilibrium between $Pu(IV)_s$ and $Pu(III)_{aq}$ (green), $Pu(V)_{aq}$ (orange) and $Pu(VI)_{aq}$ (blue). The borderlines of the stability field of water at $(pe + pH_m) = 20.77$ and $(pe + pH_m) = 0$, the "redox-neutral" line at $(pe + pH_m) = 13.8$ and the lines at $(pe + pH_m) = 1.54$ and 9 are shown for comparison.

Table A1
Thermodynamic data (at reference state) used for the equilibrium calculations of plutonium.

Chemical equilibrium	log K°
Redox reactions	
$Pu^{3+} \leftrightarrow Pu^{4+} + e^-$	–(17.69 ± 0.04) [a]
$Pu^{3+} + 2\ H_2O(l) \leftrightarrow PuO_2(am,hyd) + 4\ H^+ + e^-$	–(15.36 ± 0.52) [a]
$Pu^{4+} + 2\ H_2O(l) \leftrightarrow PuO_2^{+} + 4\ H^+ + e^-$	–(17.45 ± 0.69) [a]
$PuO_2^{+} \leftrightarrow PuO_2^{2+} + e^-$	–(15.82 ± 0.09) [a]
$PuO_2(am,hyd) \leftrightarrow PuO_2^{+} + e^-$	–(19.78 ± 0.09) [a]
Solubility and hydrolysis of Pu(III)	
$Pu(OH)_3(am) \leftrightarrow Pu^{3+} + 3\ OH^-$	–(26.2 ± 1.5) [b] [c]
$Pu^{3+} + OH^- \leftrightarrow Pu(OH)^{2+}$	(7.1 ± 0.3) [a] [d]
$Pu^{3+} + 2\ OH^- \leftrightarrow Pu(OH)_2^{+}$	(12.9 ± 0.7) [a] [d]
$Pu^{3+} + 3\ OH^- \leftrightarrow Pu(OH)_3^{0}(aq)$	(15.8 ± 0.5) [a] [d]
Solubility and hydrolysis of Pu(IV)	
$PuO_2(am, hyd) \leftrightarrow Pu^{4+} + 4\ OH^-$	–(58.33 ± 0.52) [a]
$PuO_2(cry) \leftrightarrow Pu^{4+} + 4\ OH^-$	–(64.03 ± 0.51) [a]
$Pu^{4+} + OH^- \leftrightarrow Pu(OH)^{3+}$	(14.6 ± 0.2) [a]
$Pu^{4+} + 2\ OH^- \leftrightarrow Pu(OH)_2^{2+}$	(28.6 ± 0.3) [a]
$Pu^{4+} + 3\ OH^- \leftrightarrow Pu(OH)_3^{+}$	(39.7 ± 0.4) [a]
$Pu^{4+} + 4\ OH^- \leftrightarrow Pu(OH)_4^{0}(aq)$	(47.5 ± 0.5) [a]
Solubility and hydrolysis of Pu(V)	
$PuO_2OH(am) \leftrightarrow PuO_2^{+} + OH^-$	–(9.0 ± 0.5) [a]
$PuO_{2.5}(s,hyd) \leftrightarrow PuO_2^{+} + OH^-$	–(14.0 ± 0.5) [a]
$PuO_2^{+} + OH^- \leftrightarrow PuO_2OH^0(aq)$	(2.7 ± 0.7) [a] [e]
$PuO_2^{+} + 2\ OH^- \leftrightarrow PuO_2(OH)_2^{-}$	(4.4 ± 0.5) [a] [e]
Solubility and hydrolysis of Pu(VI)	
$PuO_2(OH)_2{\cdot}H_2O(s) \leftrightarrow PuO_2^{2+} + 2\ OH^- + H_2O(l)$	–(22.5 ± 1.0) [a]
$PuO_2^{2+} + OH^- \leftrightarrow PuO_2(OH)^{+}$	(8.5 ± 0.5) [a]

(*continued on next page*)

Table A1 (*continued*)

Chemical equilibrium	log K°
$PuO_2^{2+} + 2\ OH^- \leftrightarrow PuO_2(OH)_2^0(aq)$	(14.8 ± 1.5) [a)]
$PuO_2^{2+} + 3\ OH^- \leftrightarrow PuO_2(OH)_3^-$	(21.7 ± 0.4) [a)]
$2\ PuO_2^{2+} + 2\ OH^- \leftrightarrow (PuO_2)_2(OH)_2^{2+}$	(20.5 ± 1.0) [a)]

[a)] adapted from Neck et al. (2007) and Guillaumont et al. (2003).
[b)] taken from Guillaumont et al. (2003).
[c)] value is originally reported in Felmy et al. (1989), but with an assigned uncertainty of ± 0.8 in $\log_{10}$-units.
[d)] in analogy with Am(III).
[e)] in analogy with Np(V).

Table A2
Complementary thermodynamic data (at reference state), used for the equilibrium calculations for Ca(II) under aqueous conditions.

Chemical equilibrium	log K°	Reference
$Ca^{2+} + OH^- \Leftrightarrow Ca(OH)^+$	1.22	(Blanc et al., 2010)
$Ca^{2+} + 2OH^- \Leftrightarrow Ca(OH)_2(s)$	−5.19	(Blanc et al., 2010)

Table A3
Thermodynamic data (at reference state or otherwise indicated) for the system Ca(II)–OH–ISA reported in the literature and considered in the present work.

Chemical equilibrium	log K°	Reference
$HISA(aq) \leftrightarrow HISA_L(aq) + H_2O(l)$	(0.5 ± 0.2)[a]	(Rai & Kitamura, 2015)
$H^+ + ISA^- \leftrightarrow HISA(aq)$	(3.3 ± 0.2)[a]	(Rai & Kitamura, 2015)
$H^+ + ISA\_H^{2-} \leftrightarrow ISA^-$	14.31 (I ~ 2 M)	(Evans, 2003)
$Ca^{2+} + 2\ ISA^- \leftrightarrow Ca(ISA)_2(s)$	(6.4 ± 0.2)	(Hummel et al., 2005)
$Ca^{2+} + ISA^- \leftrightarrow CaISA^+$	(1.7 ± 0.3)	(Hummel et al., 2005)
$Ca^{2+} + ISA^- \leftrightarrow CaOHISA(aq)$[b] $+ H^+$	–(10.4 ± 0.5)	(Hummel et al., 2005)

[a)] uncertainties estimated in Hummel et al. (2005).
[b)] Hummel and co-workers reported this species as $Ca(ISA\_H)(aq)$ (Hummel et al., 2005).

Table A4
Chemical equilibria and related equilibrium constants (at I → 0 m) derived in our previous study for the Pu (III/IV)–OH–ISA system (Tasi et al., 2018a).

Chemical equilibrium	log*β°
$Pu^{4+}(aq) + ISA^- + 3\ H_2O(l) \Leftrightarrow Pu(IV)(OH)_3ISA\_H^- + 4\ H^+$	–(5.03 ± 0.12)
$Pu^{4+}(aq) + ISA^- + 3\ H_2O(l) \Leftrightarrow Pu(IV)(OH)_3ISA\_2H^{2-} + 5\ H^+$	–(16.92 ± 0.13)
$Pu^{3+}(aq) + ISA^- + H_2O(l) \Leftrightarrow Pu(III)(OH)ISA\_H(aq) + 2\ H^+$	–(10.97 ± 0.28)

Table A5
Ion interaction coefficients of aqueous species in NaCl solutions.

Species i	Species j	ε(i,j) [kg·mol^{-1}]	Reference
H^+	Cl^-	0.12 ± 0.01	(Guillaumont et al., 2003)
Na^+	Cl^-	0.03 ± 0.01	(Guillaumont et al., 2003)
Na^+	OH^-	0.04 ± 0.01	(Guillaumont et al., 2003)
Na^+	ISA^-	−0.07 [a)]	(Colàs et al., 2011)
Ca^{2+}	Cl^-	0.14 ± 0.01	(Guillaumont et al., 2003)
Pu^{3+}	Cl^-	0.23 ± 0.02	(Neck et al., 2009)
$Pu(OH)^{2+}$	Cl^-	−0.04 ± 0.07	(Neck et al., 2009)

(*continued on next page*)

Table A5 (*continued*)

Species i	Species j	ε(i,j) [kg·mol^{-1}]	Reference
$Pu(OH)_2^{+}$	Cl^-	−0.06 ± 0.08	(Neck et al., 2009)
$Pu(OH)_3^0$(aq)	Cl^-	0.00	[b]
$Pu(OH)_3^0$(aq)	Na^+	−0.17 ± 0.10	(Neck et al., 2009)
Pu^{4+}	Cl^-	0.4 ± 0.1	(Neck & Kim, 2001)
$PuOH^{3+}$	Cl^-	0.2 ± 0.1	(Neck & Kim, 2001)
$Pu(OH)_2^{2+}$	Cl^-	0.1 ± 0.1	(Neck & Kim, 2001)
$Pu(OH)_3^{+}$	Cl^-	0.05 ± 0.1	(Neck & Kim, 2001)
$Pu(OH)_4^0$(aq)	Na^+/Cl^-	0.00	[b]
$Pu(IV)(OH)_3ISA_{-H}^-$	Na^+	–(0.05 ± 0.10)	[c]
$Pu(IV)(OH)_3ISA_{-2H}^{2-}$	Na^+	–(0.10 ± 0.10)	[c]
Pu(III)(OH)ISA_{-H}(aq)	Na^+/Cl^-	0.00	[b]
PuO_2^{+}	Cl^-	0.09 ± 0.05[d]	(Guillaumont et al., 2003)
PuO_2OH(aq)	Na^+/Cl^-	0.00	[b]
$PuO_2(OH)_2^-$	Na^+	−0.01 ± 0.07[d]	(Guillaumont et al., 2003)
PuO_2^{2+}	Cl^-	0.21 ± 0.02 [e]	(Guillaumont et al., 2003)
PuO_2OH^{+}	Cl^-	0.05 ± 0.1 [e]	(Hummel, 2009)
$PuO_2(OH)_2$(aq)	Na^+/Cl^-	0.00	[b]
$PuO_2(OH)_3^-$	Na^+	−0.09 ± 0.05 [f]	(Gaona, Fellhauer, & Altmaier, 2013)
$(PuO_2)_2(OH)_2^{2+}$	Cl^-	0.69 ± 0.07 [e]	(Guillaumont et al., 2003)

[a] In analogy with ε(Na+, Hox−) reported in (Rand et al., 2009).
[b] by definition in SIT.
[c] reported in Tasi et al. (2018a), values based on the work of Hummel (2009).
[d] in analogy with Np(V).
[e] in analogy with U(VI).
[f] in analogy with Np(VI).

References

Ahlrichs, R., Furche, F., Grimme, S., 2000. Comment on "Assessment of exchange correlation functionals". Chem. Phys. Lett. 325 (1–3), 317–321.

Ahlrichs, R., Furche, F., Hättig, C., Klopper, W.M., Sierka, M., Weigend, F., 2015. TURBOMOLE v7.0. University of Karlsruhe and Forschungszentrum Karlsruhe GmbH, Karlsruhe, Germany.

Altmaier, M., Neck, V., Fanghänel, T., 2008. Solubility of Zr(IV), Th(IV) and Pu(IV) hydrous oxides in CaCl2 solutions and the formation of ternary Ca-M(IV)-OH complexes. Radiochim. Acta 96(b) Baldridge, K.; Klamt A. J. Chem. Phys. 106, 6622.

Berner, U., 1992. Evolution of pore water chemistry during degradation of cement in a radioactive waste repository environment. Waste Manag. 12, 201–219.

Bernhard, G., Geipel, G., Reich, T., Brendler, V., Amayri, S., Nitsche, H., 2001. Uranyl(VI) carbonate complex formation: validation of the Ca2UO2(CO3)3(aq.) species. Radiochim. Acta 89, 511–518.

Blanc, P., Bourbon, X., Lassin, A., Gaucher, E.C., 2010. Chemical model for cement-based materials: temperature dependence of thermodynamic functions for nanocrystalline and crystalline C–S–H phases. Cement Concr. Res. 40, 851–866.

Bouby, M., Geckeis, H., Lützenkirchen, J., Mihai, S., Schäfer, T., 2011. Interaction of bentonite colloids with Cs, Eu, Th and U in presence of humic acid: a flow field-flow fractionation study. Geochem. Cosmochim. Acta 75, 3866–3880.

Brendebach, B., Banik, N.L., Marquardt, C.M., Rothe, J., Denecke, M., Geckeis, H., 2009. X-ray absorption spectroscopic study of trivalent and tetravalent actinides in solution at varying pH values. Radiochim. Acta 97, 701–708.

Colàs, E., 2014. Complexation of Th(IV) and U(VI) by Polyhydroxy and Polyamino Carboxylic Acids. Universitat Politècnica de Catalunya (UPC), Barcelona, Spain PhD Thesis.

Colàs, E., Grivé, M., Rojo, I., Duro, L., 2011. Solubility of ThO2·xH2O(am) in the presence of gluconate. Radiochim. Acta 99, 269–273.

Deglmann, P., May, K., Furche, F., Ahlrichs, R., 2004. Nuclear second analytical derivative calculations using auxiliary basis set expansions. Chem. Phys. Lett. 384, 103–107.

Dudas, C., Kutus, B., Boszormenyi, E., Peintler, G., Kele, Z., Palinko, I., Sipos, P., 2017. Comparison of the Ca2+ complexing properties of isosaccharinate and gluconate - is gluconate a reliable structural and functional model of isosaccharinate? Dalton Trans. 46, 13888–13896.

Eichkorn, K., Treutler, O., Öhm, H., Ahlrichs, H.M., Ahlrichs, R., 1995. Auxiliary basis sets to approximate Coulomb potentials. Chem. Phys. Lett. 242, 652–660.

Eichkorn, K., Weigend, F., Treutler, O., Ahlrichs, R., 1997. Auxiliary basis sets for main row atoms and transition metals and their use to approximate coulomb potentials. Theor. Chem. Acc 97, 119–124.

Endrizzi, F., Rao, L., 2014. Chemical speciation of uranium(VI) in marine environments: complexation of calcium and magnesium ions with [(UO2)(CO3)3]4 and the effect on the extraction of uranium from seawater. Chem. Eur J. 20, 14499–14506.

Evans, N., 2003. Studies on Metal A-Isosaccharinic Acid Complexes. Loughborough University, Loughborough, UK.

Fellhauer, D., Neck, V., Altmaier, M., Lützenkirchen, J., Fanghaenel, T., 2010. Solubility of tetravalent actinides in alkaline CaCl2 solutions and formation of Ca-4 An(OH)(8)(4+) complexes: a study of Np(IV) and Pu(IV) under reducing conditions and the systematic trend in the An(IV) series. Radiochim. Acta 98, 541–548.

Fellhauer, D., Altmaier, M., Gaona, X., Lützenkirchen, J., Fanghaenel, T., 2016a. Np(V) solubility, speciation and solid phase formation in alkaline CaCl2 solutions. Part II: thermodynamics and implications for source term estimations of nuclear waste disposal. Radiochim. Acta 104, 381–397.

Fellhauer, D., Rothe, J., Altmaier, M., Neck, V., Runke, J., Wiss, T., Fanghaenel, T., 2016b. Np(V) solubility, speciation and solid phase formation in alkaline CaCl2 solutions. Part I: experimental results. Radiochim. Acta 104, 355–379.

Felmy, A.R., Rai, D., Schramke, J.A., Ryan, J.L., 1989. The solubility of plutionium hydroxide in dilute solution and in high-ionic-strenght cloride brines. Radiochim. Acta 48, 29–35.

Gaona, X., Montoya, V., Colàs, E., Grivé, M., Duro, L., 2008. Review of the complexation of tetravalent actinides by ISA and gluconate under alkaline to hyperalkaline conditions. J. Contam. Hydrol. 102, 217–227.

Gaona, X., Fellhauer, D., Altmaier, M., 2013. Thermodynamic description of Np(VI) solubility, hydrolysis, and redox behavior in dilute to concentrated alkaline NaCl solutions. Pure Appl. Chem. 85, 2027–2049.

Gaona, X., Altmaier, M., Geckeis, H., 2017. Impact of Organic Ligands on the Solubility of Actinides under Repository-relevant PH/Eh Conditions, 16th International Conference on the Chemistry and Migration Behaviour of Actinides and Fission Products in the Geosphere (Book of Abstracts), Barcelona, Spain.

Gugau, K., 2016. Complexation of Nd(III) and Cm(III) with Alpha-D-isosaccharinic Acid under Repository Relevant Conditions (Master Thesis). Karlsruhe Institute of Technology, Institute for Nuclear Waste Disposal, Karlsruhe, Germany.

Guillaumont, R., Fanghänel, T., Neck, V., Fuger, J., Palmer, D.A., Grenthe, I., Rand, M.H., 2003. Update on the Chemical Thermodynamics of Uranium, Neptunium, Plutonium, Americium and Technetium. Elsevier, North Holland, Amesterdam.

Hohenberg, P., Kohn, W., 1964. Inhomogeneous electron gas. Phys. Rev. 136, B864–B871.

Hummel, W., 2009. Ionic Strength Corrections and Estimation of SIT Ion Interaction Coefficients. PSI Technical Report, TM-44-09-01. Paul Scherrer Institut, Villigen, Switzerland.

Hummel, W., Anderegg, G., Rao, L., Puigdomenech, I., Tochiyama, O., 2005. Chemical Thermodynamics of Compounds and Complexes of U, Np, Pu, Am, Tc, Se, Ni and Zr with Selected Organic Ligands. Elsevier, North-Holland, Amsterdam.

Kalmykov, S.N., Choppin, G.R., 2000. Mixed Ca2+/UO22+/CO32-complex formation at different ionic strengths. Radiochim. Acta 88, 603–608.

Keith-Roach, M., Lindgren, M., Källström, K., 2014. Assessment of Complexing Agent Concentrations in SFR. Swedish Nuclear Fuel and Waste Management Co, Stockholm, Sweden.

Klamt, A., 1995. Conductor-like screening model for real solvents: a new approach to the quantitative calculation of solvation phenomena. J. Phys. Chem. 99, 2224–2235.
Klamt, A., Schuurmann, G., 1997. Chem Soc Perkin Trans 2 (5), 799 1993.
Kohn, W., Sham, L.J., 1965. Self-consistent Equations including exchange and correlation effects. Phys. Rev. 140, A1133–A1138.
Lee, J.-Y., Yun, J.-I., 2013. Formation of ternary CaUO2(CO3)(3)(2-) and Ca2UO2(CO3)(3)(aq) complexes under neutral to weakly alkaline conditions. Dalton Trans. 42, 9862–9869.
Moritz, A., Cao, X., Dolg, M., 2007. Quasirelativistic energy-consistent 5f-in-core pseudopotentials for divalent and tetravalent actinide elements. Theoretical Chemistry Accounts 118, 845–854.
Neck, V., Kim, J.I., 2001. Solubility and hydrolysis of tetravalent actinides. Radiochim. Acta 89, 1–16.
Neck, V., Altmaier, M., Fanghänel, T., 2007. Solubility of plutonium hydroxides/hydrous oxides under reducing conditions and in the presence of oxygen. Compt. Rendus Chem. 10, 959–977.
Neck, V., Altmaier, M., Rabung, T., Lützenkirchen, J., Fanghänel, T., 2009. Thermodynamics of trivalent actinides and neodymium in NaCl, MgCl2, and CaCl2 solutions: solubility, hydrolysis, and ternary Ca-M(III)-OH complexes. Pure Appl. Chem. 81, 1555–1568.
Rai, D., Kitamura, A., 2015. Evaluation of equilibrium constants for deprotonation and lactonisation of α-D-isosaccharinic acid. J. Nucl. Sci. Technol. 53, 459–467.
Rai, D., Rao, L., Xia, Y., 1998. Solubility of crystalline calcium isosaccharinate. J. Solut. Chem. 27, 1109–1122.
Rai, D., Hess, N.J., Xia, Y.X., Rao, L., Cho, H.M., Moore, R.C., Van Loon, L.R., 2003. Comprehensive thermodynamic model applicable to highly acidic to basic conditions for isosaccharinate reactions with Ca(II) and Np(IV). J. Solut. Chem. 32, 665–689.
Rand, M., Fuger, J., Grenthe, I., Neck, V., Rai, D., 2009. Chemical Thermodynamics of Thorium. Elsevier, North-Holland, Amsterdam.
Randall, M., Rigby, B., Thomson, O., Trivedi, D., 2013. Assessment of the Effects of Cellulose Degradation Products on the Behaviour of Europium and Thorium. National Nuclear Laboratory. Chadwick House, Warington, UK.
Schäfer, A., Horn, H., Ahlrichs, R., 1992. Fully optimized contracted Gaussian basis sets for atoms Li to Kr. J. Chem. Phys. 97, 2571–2577.
Tasi, Á., Gaona, X., Fellhauer, D., Böttle, M., Rothe, J., Dardenne, K., Polly, R., Grive, M., Colas, E., Bruno, J., Kallstrom, K., Altmaier, M., Geckeis, H., 2018a. Thermodynamic description of the plutonium - alpha-D-isosaccharinic acid system I: solubility, complexation and redox behavior. Appl. Geochem (Accepted Manuscript). https://doi.org/10.1016/j.apgeochem.2018.04.014.
Tasi, Á., Gaona, X., Fellhauer, D., Böttle, M., Rothe, J., Dardenne, K., Schild, D., Grive, M., Colas, E., Bruno, J., Kallstrom, K., Altmaier, M., Geckeis, H., 2018b. Redox behavior and solubility of Plutonium under alkaline, reducing conditions. Radiochim. Acta 106, 259–279.
Taylor, H.F.W., 1997. Cement Chemistry. Thomas Telford, London (UK).
Tits, J., Wieland, E., Bradbury, M.H., Eckert, P., Schaible, A., 2002. The Uptake of Eu(III) and Th(IV) by Calcite under Hyperalkaline Conditions. Paul Scherrer Insitut, Villigen, Switzerland.
Tits, J., Wieland, E., Bradbury, M.H., 2005. The effect of isosaccharinic acid and gluconic acid on the retention of Eu(III), Am(III) and Th(IV) by calcite. Appl. Geochem. 20, 2082–2096.
Treutler, O., Ahlrichs, R., 1995. Efficient molecular numerical integration schemes. J. Chem. Phys. 102, 346–354.
Van Loon, L.R., Glaus, M.A., Vercammen, K., 1999. Solubility products of calcium isosaccharinate and calcium gluconate. Acta Chem. Scand. 53, 235–240.
Van Loon, L.R., Glaus, M.A., Vercammen, K., 2004. Stability of the ion pair between Ca2+ and 2-(Hydroxymethyl)-3-Deoxy-D-erythro-Pentonate (α-Isosaccharinate). J. Solut. Chem. 33, 1573–1583.
Vercammen, K., 2000. Complexation of Calcium, Thorium and Europium by A-Isosaccharinic Acid under Alkaline Conditions. Swiss Federal Institute of Technology, Zurich, Switzerland.
Vercammen, K., Glaus, M.A., Van Loon, L.R., 1999a. Complexation of calcium by α-isosaccharinic acid under alkaline conditions. Acta Chem. Scand. 53, 241–246.
Vercammen, K., Glaus, M.A., Van Loon, L.R., 1999b. Evidences for the existence of complexes between Th(IV) and α-isosaccharinic acid under alkaline conditions. Radiochim. Acta 84, 221–224.
Vercammen, K., Glaus, M.A., Van Loon, L.R., 2001. Complexation of Th(IV) and Eu(III) by alpha-isosaccharinic acid under alkaline conditions. Radiochim. Acta 89, 393–401.
von Arnim, M., Ahlrichs, R., 1999. Geometry optimization in generalized natural internal coordinates. J. Chem. Phys. 111, 9183–9190.
Weng, L., Temminghoff, E.J.M., van Riemsdijk, W.H., 2002. Interpretation of humic acid coagulation and soluble soil organic matter using a calculated electrostatic potential. Eoropean Journal of Soil Science 53, 575–587.
Wieland, E., Van Loon, L.R., 2002. Cementitious near-field sorption data base for performance assessment of an ILW repository in opalinus clay. PSI-Bericht 03–06 Paul Scherrer Institut, CH-5232 Villigen PSI, Switzerland.
Wieland, E., Tits, J., Dobler, J.P., Spieler, P., 2002. The effect of α-isosaccharinic acid on the stability of and Th(IV) uptake by hardened cement paste. Radiochim. Acta 90, 683–688.
Zachariansen, W.H., 1949. Crystal chemical studies of the 5f-series of elements. Xii. New compounds representing known structure types. Acta Crystallogr. 2, 388–390.